Nano-Micro Letters

ISSN 2311-6706
e-ISSN 2150-5551
CN 31-2103/TB

REVIEW

https://doi.org/10.1007/s40820-019-0309-6

Cite as
Nano-Micro Lett.
(2019) 11:79

Received: 13 July 2019
Accepted: 25 August 2019

2D MXenes as Co-catalysts in Photocatalysis: Synthetic Methods

Yuliang Sun[1,2], Xing Meng[1,2,3] ✉, Yohan Dall'Agnese[4], Chunxiang Dall'Agnese[1], Shengnan Duan[1,2], Yu Gao[1,2], Gang Chen[1,2], Xiao-Feng Wang[1,2] ✉

✉ Xing Meng, mengxing@jlu.edu.cn; Xiao-Feng Wang, xf_wang@jlu.edu.cn

1 Key Laboratory of Physics and Technology for Advanced Batteries (Ministry of Education), College of Physics, Jilin University, Changchun 130012, People's Republic of China

2 Jilin Key Engineering Laboratory of New Energy Materials and Technologies, Jilin University, Changchun 130012, People's Republic of China

3 A. J. Drexel Nanomaterials Institute and Department of Materials Science and Engineering, Drexel University, Philadelphia, PA 19104, USA

4 Institute for Materials Discovery, Faculty of Maths and Physical Sciences, University College London, London WC1E 7JE, UK

HIGHLIGHTS

- Two-dimensional transition metal carbides/nitrides (MXenes) as co-catalysts were summarized and classified according to the different synthesis methods used: mechanical mixing, self-assembly, in situ decoration, and oxidation.
- The working mechanism for MXenes application in photocatalysis was discussed. The improved photocatalytic performance was attributed to enhancement of charge separation and suppression of charge recombination.

ABSTRACT Since their seminal discovery in 2011, two-dimensional (2D) transition metal carbides/nitrides known as MXenes, that constitute a large family of 2D materials, have been targeted toward various applications due to their outstanding electronic properties. MXenes functioning as co-catalyst in combination with certain photocatalysts have been applied in photocatalytic systems to enhance photogenerated charge separation, suppress rapid charge recombination, and convert solar energy into chemical energy or use it in the degradation of organic compounds. The photocatalytic performance greatly depends on the composition and morphology of the photocatalyst, which, in turn, are determined by the method of preparation used. Here, we review the four different synthesis methods (mechanical mixing, self-assembly, in situ decoration, and oxidation) reported for MXenes in view of their application as co-catalyst in photocatalysis. In addition, the working mechanism for MXenes application in photocatalysis is discussed and an outlook for future research is also provided.

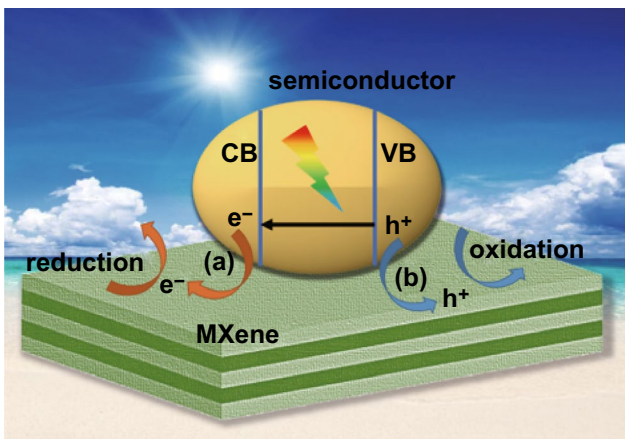

KEYWORDS MXenes; Photocatalysis; Co-catalyst; Synthetic methods

Published online: 21 September 2019

1 Introduction

Energy shortage and environmental pollution have become the two major issues faced by humanity due to limited fossil fuel resources and increasing consumption. Developing sustainable and clean energy is the key to addressing these two problems [1–15]. In being clean and inexhaustible, solar energy shows great potential to be one of the most promising future energy sources. Solar energy can be exploited in photovoltaic technologies [16], CO_2 photoreduction [17, 18], N_2 photo-fixation [19], degradation of organic compounds [20–26], and photocatalytic water splitting [27]. In renewable hydrogen fuel-based photocatalytic water-splitting systems [28–30], photocatalysts play a critical role [31, 32]. Photo-catalyzed solar energy conversion can be divided into three steps: (1) light absorption, (2) charge separation and transfer, and (3) surface reaction. Any improvement on each of these steps will contribute to enhancing the total conversion efficiency. Conventional photocatalysts such as TiO_2, g-C_3N_4, and CdS demonstrate low photocatalytic efficiency due to rapid charge recombination in these materials. Using noble metals such as Pt, Ru, and Pd as co-catalysts will increase cost, although such materials can enhance charge separation ability and suppress recombination of charges. A co-catalyst that is both efficient and cheap is thus urgently needed to promote the development of photocatalysis.

MXenes, comprising transition metal carbides, nitrides, and carbonitrides, are a new family of two-dimensional (2D) materials that have attracted much attention in recent years [2]. The general formula of MXene is $M_{n+1}X_n$ ($n = 1, 2, 3$), where M represents a transition metal, such as Sc, Ti, Zr, Hf, V, Nb, Ta, and Mo, while X represents C and/or N. Owing to their unique structure and superior photoelectronic properties, layered structure MXenes show various potential applications in different areas, such as energy storage [3, 33–38], electromagnetic interference shielding [39, 40], gas sensors [41], wireless communication [42], water treatment [43, 44], solar cells [45–47], and catalysis [41, 48–51]. 2D MXenes are being increasingly studied in the past few years, as evidenced by the rapidly increasing number of scientific articles published per year (Fig. 1a). MXenes are usually synthesized by selectively etching the A layer from MAX phases, which constitute a family of tertiary ductile ceramics, where the A layer is made of an element such as Al, Ga [52], or Si [53]. After selective etching of the A layer, 2D MX layers with surface functional groups (–O, –OH, –F, or a mixture of several groups denoted as T_x) are left. The most widely used methods for selective etching are wet chemical HF etching and in situ HF etching (using a mixture of acids and fluoride salts), although other routes using tetramethylammonium hydroxide (TMAOH) [54, 55], electrochemical [56, 57], or etching with NaOH [58], and $ZnCl_2$ [49]) have also been explored. Generally, multilayered MXenes are produced by HF etching, whereas single or few-layered MXene flakes are obtained by in situ HF etching or through delamination of a multilayered MXene by intercalation of large organic molecules (Fig. 1b). The etching methods of $Ti_3C_2T_x$ MXene, which is the first discovered and the most studied MXene, have been reviewed elsewhere [59, 60].

In view of the rapid development in the application of 2D MXenes, several reviews on their synthesis [59–61], and application in energy storage [33, 48, 62] and catalysis

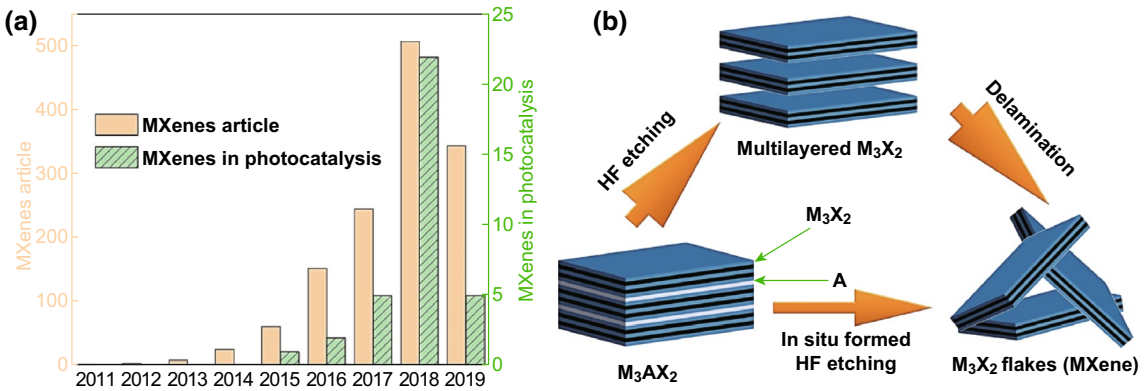

Fig. 1 **a** The rapid expansion of 2D MXenes materials and **b** the most widely used methods to synthesize MXenes

https://doi.org/10.1007/s40820-019-0309-6

[51] have been reported. MXenes are promising for application in photocatalysis [63] because of their large surface area, good conductivity, presence of a sufficient number of active sites, and containing suitable elements for effective photocatalysis, but they cannot be directly used as photocatalysts since MXenes are generally not semiconductors [51, 62]. Although there are some MXene semiconductors that have been predicted theoretically [64–68], these have not yet been experimentally synthesized. In this review, we give a detailed discussion on MXene as a co-catalyst in photocatalysis and describe the different methods used for the synthesis of MXene-derived photocatalysts, along with problems encountered in this system and a prospective outlook on future research in this field.

2 Synthetic Methods for MXenes as Co-catalysts in Photocatalysis

In view of their good conductivity and large surface area, MXenes have been applied in photocatalysis both to replace noble metal co-catalysts and to enhance the charge separation ability of the photocatalyst (Fig. 2). The most common methods used for the preparation of photocatalyst composites include mechanical mixing, self-assembly, in situ decoration and oxidation, or a combination of the three methods.

2.1 Mechanical Mixing and Self-assembly

Mechanical mixing is the easiest method to form photocatalyst composites. Stirring the two components in the liquid phase or grinding of powders can be used for sample preparation. Interestingly, due to electrostatic attraction, photocatalysts with positive charge are easily combined with MXenes whose surfaces are enriched with negative charges, leading to self-assembled photocatalyst composites. In addition, the self-assembling property could be further improved by using other induced techniques simultaneously, where the photocatalysts and co-catalysts are prepared in advance [44].

An et al. [72] demonstrated that synergetic effects of Ti_3C_2 MXene and Pt when used as dual co-catalysts enhanced the photoactivity of g-C_3N_4 for hydrogen evolution (Fig. 3a), where HF-etched exfoliated Ti_3C_2 and g-C_3N_4 were mixed in liquid by stirring followed by photodeposition of Pt on the composites. The photoactivity of the dual

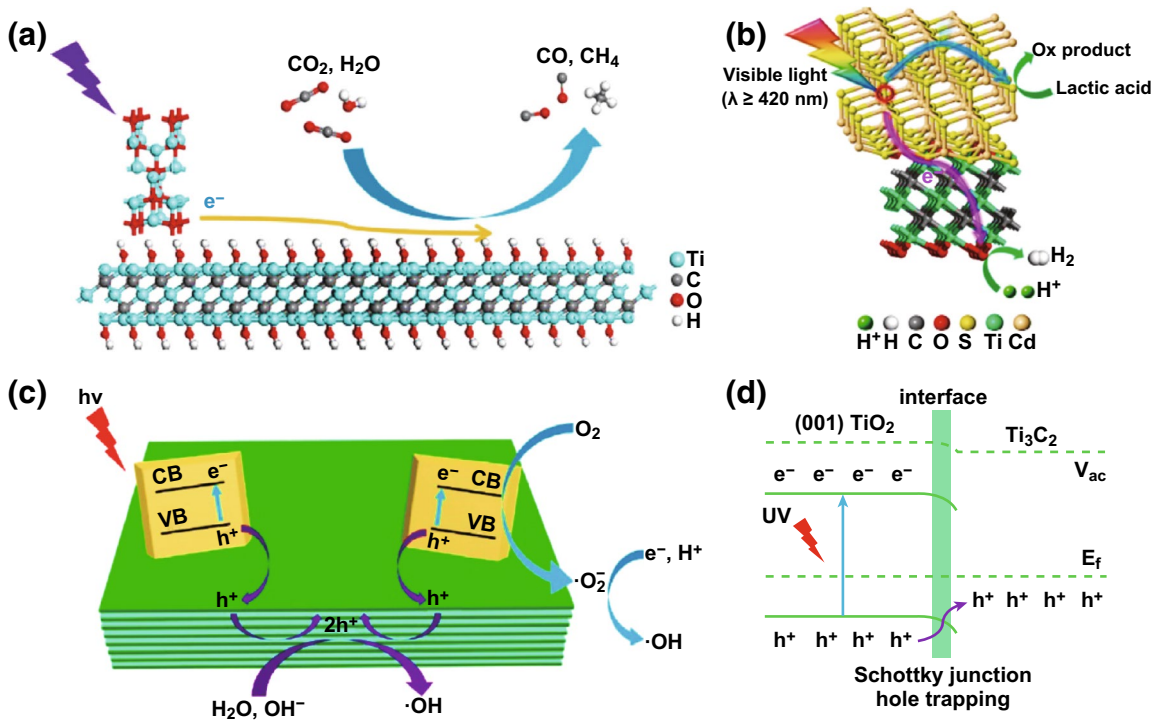

Fig. 2 Schematic showing charge separation between MXene co-catalyst and a photocatalyst taken from **a** Ye et al. Reprinted with permission from Ref. [69]. Copyright 2018 John Wiley & Sons. **b** Ran et al. Reprinted with permission from Ref. [70]. Copyright 2017 Nature Publishing Group. **c**, **d** Peng et al. Reprinted with permission from Ref. [71]. Copyright 2016 American Chemical Society

co-catalysts-modified photocatalysts (g-C_3N_4/Ti_3C_2/Pt) was much better than that of Pt- or Ti_3C_2-only systems, reaching 5.1 mmol h^{-1} g^{-1} in hydrogen production (Fig. 4a). This enhanced performance was due to the presence of Ti_3C_2 MXene that facilitated interfacial charge separation and carrier transport from the conduction band (CB) of g-C_3N_4 to Pt. Our group prepared g-C_3N_4/$Ti_3C_2T_x$ composites by grinding g-C_3N_4 and $Ti_3C_2T_x$ powders together followed by annealing in different gas atmospheres, to tune the surface termination groups (Fig. 4b) [74]. X-ray photoelectron spectroscopy data showed an increase in –O termination groups accompanied by a decrease in –F termination groups on the surface of Ti_3C_2. Ti_3C_2 with –O termination groups had better photoactivity, revealing that the presence of such groups in Ti_3C_2 had a positive effect on hydrogen production by increasing the number of active sites. Moreover, this finding was consistent with density functional theory (DFT) simulation results. The $|\Delta G_H|$ of Ti_3C_2 with –O terminations was found to be as low as 0.01 eV, which is lower than that of Pt (111). In a similar study, Ye et al. [69] treated HF-etched Ti_3C_2 with KOH to convert –F groups into –OH groups, and then combined the KOH-treated Ti_3C_2 with TiO_2 (P25) powder by stirring in water (Fig. 3c). DFT calculations demonstrated that –OH groups played the role of active sites for the adsorption and activation of CO_2 reduction [69]. Experimentally, the photoactivities for CO_2 reduction were increased 3 times and 277 times after KOH treatment, for CO and CH_4, respectively (Fig. 4d). Interestingly, increasing the number of –OH groups not only improved the photo-conversion efficiency but also changed the nature of the products. The –OH groups resulting from KOH treatment provided more active sites for CO_2 adsorption and enabled greater electron transfer to CO_2 and facilitated its reduction to CH_4. Though the surface termination groups can be changed through annealing and KOH treatments, –F groups could not be completely exchanged. More studies to precisely tailor the termination groups need to be carried out in the future.

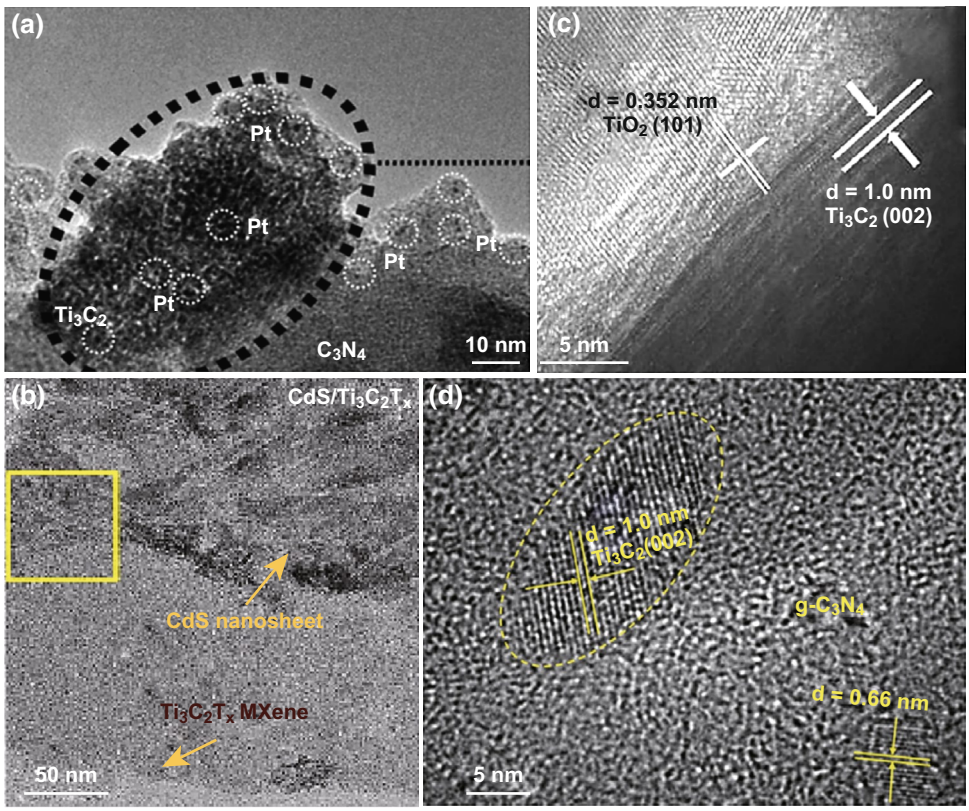

Fig. 3 TEM images of photocatalysts combined with a MXene by mechanical mixing taken from **a** An et al. Reprinted with permission from Ref. [72]. Copyright 2018 The Royal Society of Chemistry. **b** Xie et al. Reprinted with permission from Ref. [73]. Copyright 2018 Elsevier. **c** Ye et al. Reprinted with permission from Ref. [69]. Copyright 2018 John Wiley & Sons. **d** Liu et al. Reprinted with permission from Ref. [44]. Copyright 2018 Elsevier

https://doi.org/10.1007/s40820-019-0309-6

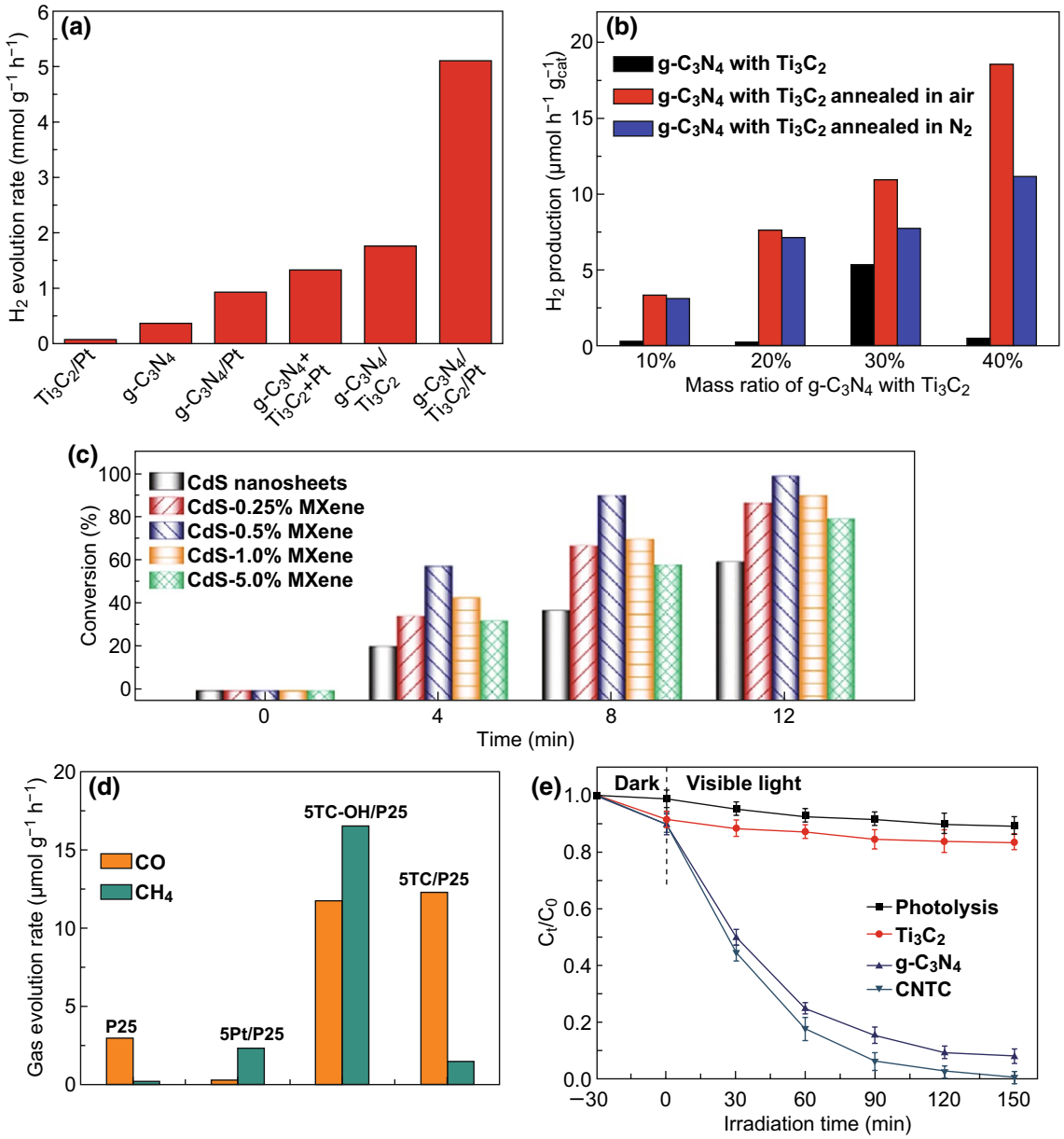

Fig. 4 Hydrogen production of different samples taken from **a** An et al. Reprinted with permission from Ref. [72]. Copyright 2018 The Royal Society of Chemistry. **b** Sun et al. Reprinted with permission from Ref. [74]. Copyright 2018 The Royal Society of Chemistry. **c** Photo-degradation of 4-nitroaniline (4-NA) over different samples from Xie et al. Reprinted with permission from Ref. [73]. Copyright 2018 Elsevier. **d** Rates of evolution of CO and CH_4 over different samples from Ye et al. Reprinted with permission from Ref. [69]. Copyright 2018 John Wiley & Sons. **e** Ciprofloxacin degradation from Liu et al. Reprinted with permission from Ref. [44]. Copyright 2018 Elsevier

Xie et al. [73] used an electrostatic self-assembly process to combine positively charged CdS nanosheets and Ti_3C_2 nanosheets (possessing negative charge) (Fig. 3b) for CO_2 reduction (Fig. 4c). Cai et al. [75] synthesized Ag_3PO_4/Ti_3C_2 by electrostatically driven self-assembly method, which had the advantage of being a mild method that prevented Ti_3C_2 from oxidation. The composites showed better performance than reduced graphene oxide (rGO), and this preparation procedure provided a new direction to the preparation of semiconductor-MXene composites. Liu et al. [44] fabricated a 2D layered and stacked g-C_3N_4/Ti_3C_2 composite by evaporation-induced self-assembly and used it to degrade

organic pollutants (ciprofloxacin) (Fig. 3d). Both photogenerated holes and superoxide radicals ($\cdot O_2^-$) resulting from photogenerated electrons played important roles in ciprofloxacin decomposition (Fig. 4f); in this process, self-assembly was an efficient method that allowed intimate mixing of the components in the composite. The sample was also more homogeneous than mechanically mixed ones because of the electrostatic attraction between the charged entities. However, opposite charges on each surface were required for self-assembly, which limited wider application of this process. Therefore, other techniques to induce self-assembly such as evaporation-induced self-assembly were developed to widen the range of application of products [44].

The above-mentioned MXene-based composites prepared by mechanical mixing and self-assembly methods for photocatalysis application are summarized in Table 1. Results from all these works prove that 2D MXene is an efficient additive material to enhance charge separation and charge transfer during photocatalysis. In these two methods, the properties of MXenes are retained by avoiding high temperature and use of other solvents or surfactant. No change in oxidation or surface termination groups occurs in these synthesis methods. Therefore, these two are the easiest and allow synthesis under the mildest conditions.

2.2 In Situ Decoration of Semiconductors onto the Surface of MXenes

In contrast to composites prepared by mechanical mixing of materials, in situ decoration methods consist in synthesizing a different material directly onto the MXene surface. As a result, in situ synthetized materials and MXenes are chemically bonded, which could be an important advantage in some designs. However, the range of viable synthetic conditions for in situ decoration is limited, because MXenes are easily oxidized in solution, especially at high temperatures [107]. It is therefore necessary to use mild conditions to protect MXenes from oxidation, especially when mono- and few-layered MXenes are used. So far, g-C_3N_4, TiO_2, CdS, and bismuth compounds have been bonded to various MXenes using this strategy.

g-C_3N_4 is one 2D semiconductor material that is combined with MXenes used as a co-catalyst in the photocatalysis process (Fig. 5). MXene can be added during the calcination of a precursor, such as melamine and thiourea, but the high calcination temperature (around 550 °C) may cause the oxidation of MXene into TiO_2. The high photoactivity of g-C_3N_4/MXene is attributed to the efficient charge separation; moreover, the heterojunction formed by TiO_2/g-C_3N_4 also plays an important role in charge separation [108]. Shao et al. [81] synthesized Ti_2C/g-C_3N_4 by melamine calcination and used it in hydrogen production (Fig. 5a, d). Though the ratio of Ti_2C in the composite was as low as 0.4 wt%, a peak due to TiO_2 resulting from the oxidation of Ti_2C could be seen in the XRD pattern. Liu et al. [19] synthesized TiO_2@C/g-C_3N_4 heterojunction by melamine calcination (Fig. 5b), where Ti_3C_2 was oxidized to TiO_2@C during the calcination process. This composite was highly effective in the reaction of nitrogen reduction to ammonia, with the best performance reaching as high as 250.6 μmol h^{-1} g^{-1}, which was better than that of TiO_2@C and g-C_3N_4 (Fig. 5e). Xu et al. [82] synthesized Ti^{3+}-rich Ti_3C_2/g-C_3N_4 by calcination of thiourea and employed it as an electrode for CO_2 reduction in a photoelectrocatalytic (PEC) system (Fig. 5c, f), achieving a total CO_2 reduction rate of 25.1 mmol h^{-1} g^{-1}. The Ti^{3+} species suppressed charge recombination at the Ti_3C_2/g-C_3N_4 heterojunctions, leading to a corresponding increase in CO_2 conversion efficiency.

Apart from the above-mentioned synthesis methods, composite photocatalysts can also be synthesized by combining TiO_2, a metal sulfide, or a bismuthide with MXene under hydrothermal conditions (Fig. 6). Gao et al. [83] synthesized TiO_2/Ti_3C_2 nanocomposites by a hydrothermal method using $TiSO_4$ as a precursor for methyl orange (MO) degradation (Fig. 6a), where small TiO_2 particles could be observed on the surface of multilayered Ti_3C_2. Wang et al. [84] employed $TiCl_4$ as the precursor in the hydrothermal synthesis of rutile TiO_2/$Ti_3C_2T_x$ for hydrogen production by water splitting (Fig. 6d). The photocatalytic activity of TiO_2 when combined with other MXenes (Ti_2CT_x and Nb_2CT_x flakes) as co-catalysts was also explored; results proved that in general, MXenes could be used as effective co-catalysts for solar hydrogen production. Ran et al. [70] combined CdS and Ti_3C_2 particles by a one-step hydrothermal reaction (Fig. 6b). A hydrogen production rate of 14,342 μmol h^{-1} g^{-1} was achieved when using Ti_3C_2 as the co-catalyst; this performance is 136.6 times higher than that of the pure CdS photocatalyst. The effectivity and versatility of Ti_3C_2 MXene as a co-catalyst for photocatalytic hydrogen production was demonstrated by other metal sulfides (ZnS) [91] photocatalysts as well. Xie et al. [73] showed that Ti_3C_2

https://doi.org/10.1007/s40820-019-0309-6

Table 1 MXene-based composites prepared by different synthetic methods for photocatalysis applications

Sample	MXene (synthetic method)	Sample synthesis	Reactant	Sacrificial agent	Rate	Precursor	Refs.
g-C_3N_4/3%Ti_3C_2/2%Pt	Ti_3C_2 flakes (HF 48%, 20 h, 60 °C and H_2O delamination, 12 h, ultrasonication)	(1) Ti_3C_2 stirring dispersions (2) Pt UV deposition	H_2O	10 vol% triethanolamine (TEOA)	5100 μmol/h/$g_{cat.}$	–	An et al. [72]
g-C_3N_4/$Ti_3C_2T_x$ (1: 0.3)	Multilayer Ti_3C_2 (HF 49%, 24 h)	Grinding in a mortar	H_2O	10 vol% TEOA	88 μmol/h/$g_{cat.}$	–	Sun et al. [74]
CdS/0.5%$Ti_3C_2T_x$	Ti_3C_2 flakes (LiF 1 g/HCl 9 M, 24 h, 35 °C)	(1) Ultrasonication (2) Stirring in water	4-NA	40 mg ammonium formate in 30 mL solution	180 mg/L/h	–	Xie et al. [73]
P25/5%Ti_3C_2-OH	Multilayer Ti_3C_2 (HF 49%, 24 h and KOH 2 M, 4 h)	Stirring in water	CO_2	–	28.35 μmol/h/$g_{cat.}$	–	Ye et al. [69]
a-Fe_2O_3/Ti_3C_2 (1: 2)	Multilayer Ti_3C_2	(1) Stirring in ethanol (2) Ultrasonication	Rhodamine B (RhB)	–	5 mg/L/h	–	Zhang et al. [76]
g-C_3N_4/Ti_3C_2 (100: 3)	Ti_3C_2 flakes (HF 40%, 24 h and H_2O intercalation, 5 h, ultrasonication)	(1) Ultrasonication (2) Stirring in water at 60 °C	Ciprofloxacin	–	18 mg/L/h	–	Liu et al. [44]
TiO_2/5%Ti_3C_2	Ti_3C_2 flakes (LiF 1 g/HCl 6 M, 24 h, 35 °C)	Sonication	H_2O	25% Methanol	2650 μmol/h/$g_{cat.}$	–	Su et al. [77]
			H_2O			–	
Ag_3PO_4/2%Ti_3C_2	Ti_3C_2 flakes (NaF 3.35 g/HCl 36–38 wt%, 12 h, 60 °C)	(1) Stirring in water with $AgNO_3$ (2) Adding Na_2HPO_4	Tetracycline hydrochloride (TC-H) etc.	–	192 mg/L/h	–	Cai et al. [75]
3%Ti_3C_2/g-C_3N_4	Ti_3C_2 flakes (LiF 1.5 g/HCl 6 M, 24 h, 35 °C)	(1) Sonication in HCl (2) Stirring	H_2O	10 vol% TEOA	73.3 μmol/h/g_{cat}	–	Su et al. [78]
TiO_2/0.5%Ti_3C_2/1% CoS_x	Multilayer Ti_3C_2 (HF 49%, 4 h)	(1) Stirring in 2-methylimidazole (2) Hydrothermal 140 °C for 12 h with thioacetamide	H_2O	20 vol% methanol	950 μmol/h/$g_{cat.}$	$Co(NO_3)_2$, 2-methylimidazole and thioacetamide	Zhao et al. [79]

Table 1 (continued)

Sample	MXene (synthetic method)	Sample synthesis	Reactant	Sacrificial agent	Rate	Precursor	Refs.
$CdS/MoS_2/2\%Ti_3C_2T_x$	Ti_3C_2 flakes (HF 49%, 72 h, ultrasonication in H_2O, 2 h)	(1) MoS_2 synthesis (2) Stirring with Ti_3C_2 (3) Add CH_4N_2S and $Cd(CH_3COO)_2$ (4) Hydrothermal 160 °C for 24 h	H_2O	0.25 M Na_2S and 0.35 M Na_2SO_3	9679 μmol/h/$g_{cat.}$	$Cd(CH_3COO)_2$, CH_4N_2S, MoS_2	Chen et al. [80]
$0.4\%Ti_2C/g\text{-}C_3N_4$	Ti_2C flakes (NH_4F 16 g/HCl 9 M, 24 h)	(1) Stirring ethanol (2) 550 °C, 4 h in muffle	H_2O	10 vol% TEOA	950 μmol/h/$g_{cat.}$	Melamine	Shao et al. [81]
$10\%TiO_2@C/g\text{-}C_3N_4$	Multilayer Ti_3C_2 (HF 49%, 4 h)	(1) Stirring in water (2) 550 °C, 2 h in muffle	N_2	20 vol% methanol	250 μmol/h/$g_{cat.}$	Melamine	Liu et al. [19]
$Pd\text{-}Ti_3C_2/g\text{-}C_3N_4$(1:10)	Multilayer Ti_3C_2 (HF 40%, 24 h)	(1) Grinding (2) 500 °C, 2 h in muffle (3) Pd electrodeposition	CO_2	0.1 M $KHCO_3$	25,100 μmol/h/$g_{cat.}$	Thiourea	Xu et al. [82]
0.001 molTiO_2/Ti_3C_2	Multilayer Ti_3C_2 (HF 49%, 24 h, 60 °C)	(1) Stirring (2) Hydrothermal 180 °C, 18 h	Methyl orange (MO)	–	40 mg/L/h	$TiSO_4$	Gao et al. [83]
$TiO_2/5\%Ti_3C_2$	Ti_3C_2 flakes (HF 48%, 15 h and DMSO delamination, 15 h)	(1) Stirring in ice-water bath (2) Heated 95 °C, 4 h	H_2O	25% methanol	43 μmol/h/$g_{cat.}$	$TiCl_4$	Wang et al. [84]
$TiO_2/5\%Ti_2C$	Ti_2C flakes (HF 10%, 10 h and DMSO delamination)						
$TiO_2/5\%Nb_2C$	Nb_2C flakes (HF 48%, 90 h and 20% isopropyl alcohol delamination)						
$CdS/2.5\%Ti_3C_2$	Ti_3C_2 nanoparticles (HF 49%, 20 h, 60 °C and H_2O delamination, ultrasonication, 5 h)	(1) Stirring in water (2) Hydrothermal 180 °C, 12 h	H_2O	Lactic acid (88 vol%)	14,342 μmol/h/g	$Cd(Ac)_2$ Thiourea	Ran et al. [70]

https://doi.org/10.1007/s40820-019-0309-6

Table 1 (continued)

Sample	MXene (synthetic method)	Sample synthesis	Reactant	Sacrificial agent	Rate	Precursor	Refs.
TiO_2/C/$BiVO_4$ (1: 1079)	Ti_3C_2 flakes (LiF 1.5 g/HCl 6 M, 48 h, 50 °C)	(1) Stirring in water (2) Hydrothermal 100 °C, 6 h	RhB	–	3.1 mg/L/h	$Bi(NO_3)_3$ NH_4VO_3	Shi et al. [85]
TiO_2/Ti_3C_2 (1: 1)	Multilayer Ti_3C_2 (HF 40%, 26 h, 60 °C)	(1) Stirring in 10 M NaOH (2) Hydrothermal 180 °C, 10 h	Methylene blue (MB)	–	8.5 mg/L/h	P25	Luo et al. [86]
BiOBr/Ti_3C_2 (250: 1)	Ti_3C_2 flakes (LiF 3 g/HCl 9 M, 24 h, 35 °C)	(1) Stirring (2) Refluxed 80 °C, 2 h	RhB	–	24 mg/L/h	$Bi(NO_3)_3$ and KBr	Liu et al. [87]
2%Ti_3C_2/Bi_2WO_6	Ti_3C_2 flakes (HF 40%, 72 h and DMSO delamination, ultrasonication, 1 h)	(1) Stirring (2) Hydrothermal 120 °C, 24 h	CO_2	–	2.22 μmol/h/$g_{cat.}$	$Bi(NO_3)_3$ Na_2WO_4	Cao et al. [88]
$Bi_{0.9}Gd_{0.1}Fe_{0.8}Sn_{0.2}O_3$/$Ti_3C_2$	Multilayer Ti_3C_2 (HF 39%, 36 h)	(1) Stirring in 0.01 M acetic acid and ethylene glycol (2) Sonicated, 2 h, 60 °C (3) stirring 1 h, 80 °C	Congo red	–	–	$Bi_{1-x}Gd_xFe_{1-y}Sn_y$	Tariq et al. [89]
In_2S_3/TiO_2@ $Ti_3C_2T_x$ (1: 0.123)	Multilayer Ti_3C_2 (HF 50%, 20 h)	(1) Stirring (2) Hydrothermal 180 °C, 24 h	MO	–	18 mg/L/h	$In(NO_3)_3$ CH_3CSNH_2	Wang et al. [90]
ZnS/0.75 wt%Ti_3C_2	Ti_3C_2 flakes (HF, 24 h, 25 °C)	(1) Stirring in ethanol–glycerol (2) Hydrothermal 180 °C, 10 h	H_2O	20 vol% lactic acid	502.6 μmol/h/$g_{cat.}$	$ZnCl_2$	Tie et al. [91]
Ti_2C/3%TiO_2/1%Ag	Multilayer Ti_2C (HF 48%)	(1) Stirring for volatiles evaporation (2) Annealing in H_2 at 400 °C	Salicylic acid	–	32.4 μmol/h	Titanium isopropylate	Wojciechowski et al. [92]

Table 1 (continued)

Sample	MXene (synthetic method)	Sample synthesis	Reactant	Sacrificial agent	Rate	Precursor	Refs.
TiO_2/Ti_3C_2 (12 h)	Multilayer Ti_3C_2 (HF 49%, 12 h, 60 °C)	Hydrothermal 160 °C for different time, $NaBF_4$ and HCl	MO	–	24 mg/L/h	–	Peng et al. [71]
TiO_2/Ti_3C_2 (20 h)	Multilayer Ti_3C_2 (HF 49%, 12 h, 60 °C)	Hydrothermal 200 °C for different time, NH_4F	MB	–	6 mg/L/h	–	Peng et al. [93]
HC-TiO_2	Ti_3C_2 flakes (tetramethylammonium hydroxide 25%, 24 h)	Hydrothermal 160 °C, 9 h	H_2O	10 vol% TEOA	33.04 μmol/h/$g_{cat.}$	–	Jia et al. [94]
4%Cu_4/TiO_2@ $Ti_3C_2T_x$-12 h	Multilayer Ti_3C_2 (HF 49%, 12 h, 60 °C)	(1) Hydrothermal 160 °C for different time, $NaBF_4$ and HCl (2) Photodepositing copper nanodots	H_2O	6.7 vol% methanol	764 μmol/h/$g_{cat.}$	–	Peng et al. [95]
Ti_3C_2/TiO_2/CuO (100:1)	Multilayer Ti_3C_2 (HF 49%, 24 h, 60 °C)	(1) Dissolved in water (2) Annealing in argon, 500 °C, 30 min	MO	–	15 mg/L/h	–	Lu et al. [96]
C/TiO_2-700 °C-150 sccm	Multilayer Ti_3C_2 (HF 40%, 90 h, 55 °C)	Heated in CO_2 at different temperature and different rate, 1 h	H_2O	10 vol% TEOA	480 μmol/h/$g_{cat.}$	–	Yuan et al. [97]
TiO_2/Ti_3C_2 (TT550 °C)	Multilayer Ti_3C_2 (HF 50%, 48 h)	Calcination at different temperature	CO_2	–	4.4 μmol/h/$g_{cat.}$	–	Low et al. [98]
Nb_2O_5/C/Nb_2C-1 h	Multilayer Nb_2C (HF 50%, 90 h)	Annealing in CO_2, 850 °C for different time	H_2O	25% methanol	7.81 μmol/h/$g_{cat.}$	–	Su et al. [99]
Microporous-MXene/ TiO_{2-x} nanodots	Multilayer Ti_3C_2 (HF 50%, 90 h)	30% H_2O_2, 10 min	RhB.etc.	–	–	–	Cheng et al. [100]
C/TiO_2	Multilayer Ti_2C (HF 40%, 2.5 h)	High-energy ball milling in air, 1.5 h, 200 rpm	MB	–	2.13 mg/L/h	–	Li et al. [101]

https://doi.org/10.1007/s40820-019-0309-6

Table 1 (continued)

Sample	MXene (synthetic method)	Sample synthesis	Reactant	Sacrificial agent	Rate	Precursor	Refs.
TiO_2/Ti_3C_2@AC-48 h	Multilayer Ti_3C_2 (HF 49%, 24 h)	Heated in H_2O for different time at 60 °C	H_2O	29 g/L ascorbic acid (AA)	33.4 μmol/h/$g_{cat.}$	–	Sun et al. [102]
Ti_3C_2/TiO_2-500/Pt	Multilayer Ti_3C_2 (HF 40%, 72 h)	(1) Hydrothermal in 1 M NaOH and 30% H_2O_2, 140 °C, 12 h (2) Immersed in 0.1 M HCl, 24 h (3) Annealing in muffle for different time	H_2O	20 vol% methanol	H_2 1596.35 μmol/h/$g_{cat.}$	–	Li et al. [103]
				0.01 M $AgNO_3$	O_2 500 μmol/h/$g_{cat.}$		
				–	H_2 526 μmol/h/$g_{cat.}$ and O_2 315 μmol/h/$g_{cat.}$		
LDC-S-TiO_2/C	Multilayer Ti_3C_2 (HF 40%, 48 h, 45 °C)	(1) Ball mixing with sulfur (2) Hydrothermal 155 °C,12 h (3) Annealing in CO_2 at 700 °C for 2 h (4) Annealing in air at 450 °C, 2 h	H_2O	10% methanol	333 μmol/h/$g_{cat.}$	–	Yuan et al. [104]
TiO_2/Ti_3C_2	Multilayer Ti_3C_2 (HF 30%, 10 h, 40 °C)	Hydrothermal 160 °C for 12 h, $NaBF_4$ and HCl	Carbamazepine	–	1.48 mg/L/h	–	Shahzad et al. [105]
Ti_3C_2/TiO_2/15%MoS_2	Multilayer Ti_3C_2 (HF 40%, 72 h)	(1) Hydrothermal 160 °C for 12 h with $NaBF_4$ and HCl (2) Hydrothermal 200 °C for 24 h with Na_2MoO_4 and CN_2H_4S	H_2O	TEOA	6425 μmol/h/$g_{cat.}$	$NaBF_4$, HCl, Na_2MoO_4 and CN_2H_4S	Li et al. [106]

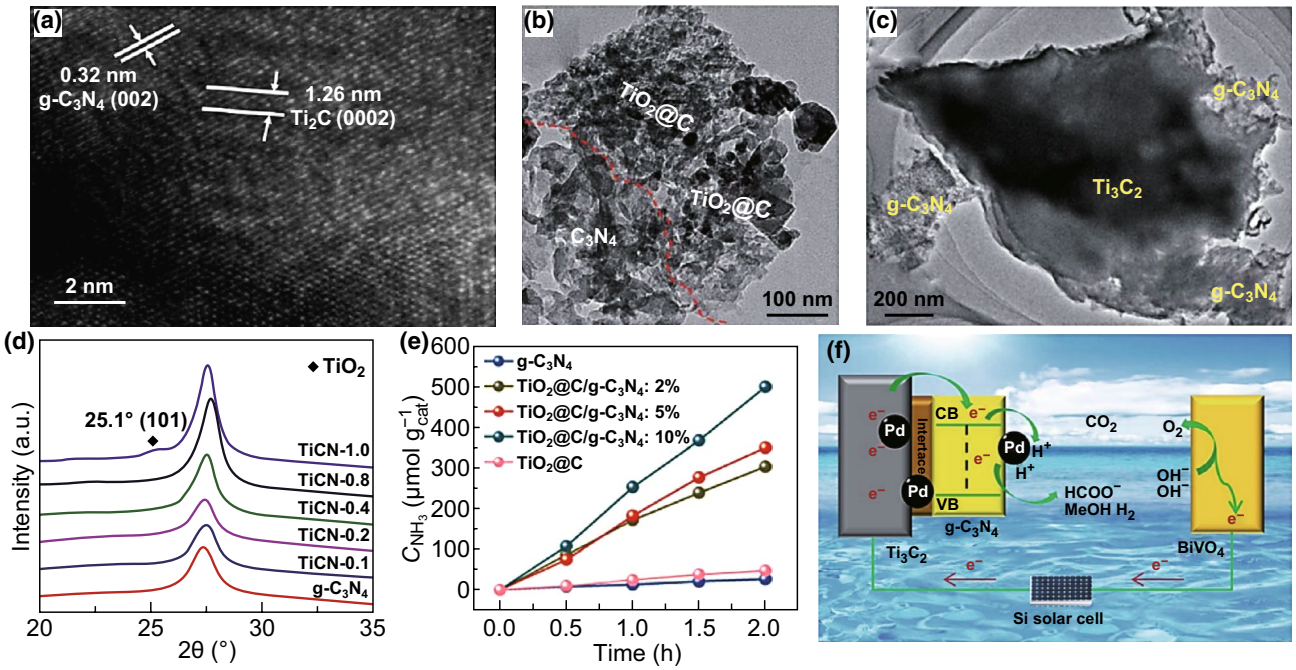

Fig. 5 Photocatalytic composites based on MXene in combination with g-C_3N_4 formed by in situ decoration. **a**–**c** TEM images, **d** XRD patterns, **e** hydrogen production, and **f** mechanism for PEC reduction of CO_2 from Shao et al. **a**, **d** Reprinted with permission from Ref. [81]. Copyright 2017 The Royal Society of Chemistry; **b**, **e** with permission from Ref. [19], Copyright 2018 The Royal Society of Chemistry; and **c**, **f** with permission from Ref. [82]. Copyright 2018 The Royal Society of Chemistry

flakes enabled the local confinement of Cd^{2+} released during photo-corrosion and thus enhanced the stability of the metal sulfide. Besides CdS, $In_2S_3/Ti_3C_2T_x$ hybrids synthesized by hydrothermal method have been used for methyl orange degradation as reported by Wang et al. [90]. Among the hybrids based on other additives (carbon nanotubes (CNT), rGO, MoS_2, and TiO_2), Ti_3C_2-based composites showed the best photocatalytic activity, which is attributed to their high electrical conductivity. Shi et al. [85] synthesized TiO_2/C/$BiVO_4$ composites by hydrothermal method for the degradation of Rhodamine B, where Ti_3C_2 was employed both as a support for the growth of $BiVO_4$ nanoparticles and as a precursor for the generation of 2D-carbon upon oxidation. The electron transfer process was accelerated by the presence of Ti_3C_2-derived 2D-carbon layers, thus improving the photocatalytic performance for Rhodamine B degradation. Ultrathin 2D/2D heterojunction of MXene/Bi_2WO_6 prepared by the in situ growth of ultrathin Bi_2WO_6 nanosheets on the surface of ultrathin Ti_3C_2 nanosheets for photocatalytic CO_2 reduction was reported by Cao et al. [88] (Fig. 6c). The CH_4 and CH_3OH yield were 4.6 times higher than those obtained with pristine Bi_2WO_6, which was ascribed to the enhanced CO_2 adsorption arising from the increased specific surface area and improved pore structure of the layered heterojunction. The different composites/hybrids containing MXene or MXene-derived products prepared by hydrothermal methods and used in photocatalysis are listed in Table 1.

The synthetic process for MXenes-based composites includes doping into the photocatalysts or using MXene as a support for in situ decoration of the semiconductor photocatalyst. The chemical reactions taking place during photocatalyst formation led to increased interfacial area, thus providing greater possibilities for the transfer of photogenerated electrons. However, one disadvantage of this method is the oxidation of MXenes during photocatalyst synthesis. Although difficult to precisely characterize, conditions of formation of the photocatalysts may be too harsh and cause structural degradation of MXenes, especially in the case of single-layered MXenes, due to their lower stability toward oxidation.

https://doi.org/10.1007/s40820-019-0309-6

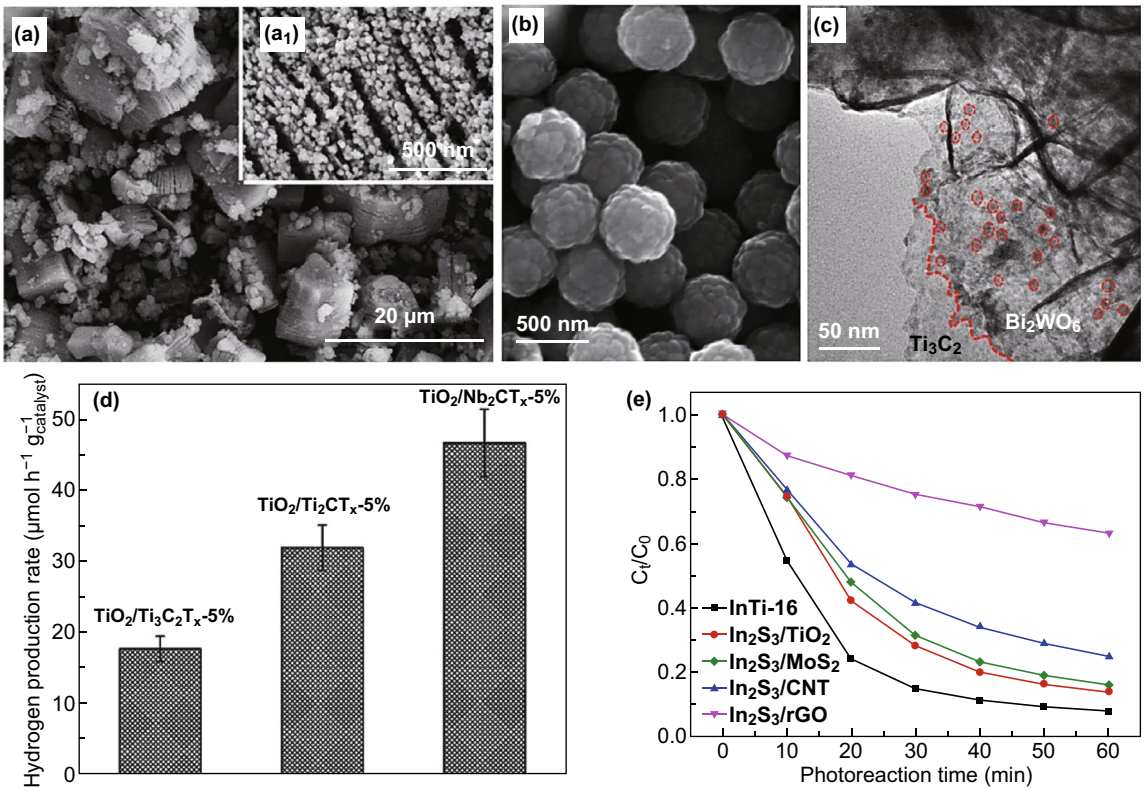

Fig. 6 Photocatalysts based on in situ decoration of MXenes. SEM images from **a** Gao et al. Reprinted with permission from Ref. [83]. Copyright 2015 Elsevier. **b** Ran et al. Reprinted with permission from Ref. [70]. Copyright 2017 Nature Publishing Group. **c** TEM images from Cao et al. Reprinted with permission from Ref. [88]. Copyright 2018 John Wiley & Sons. **d** Hydrogen production from Wang et al. Reprinted with permission from Ref. [84]. Copyright 2016 John Wiley & Sons. **e** Degradation of methyl orange (MO) from Wang et al. Reprinted with permission from Ref. [90]. Copyright 2018 Elsevier

2.3 MXene-Derived Photocatalysts

Different from mechanical mixing, self-assembly, and decoration methods, the in situ oxidation method using MXene (Ti_3C_2 is the most studied example) as a precursor for the synthesis of photocatalysts has also been explored (Fig. 7). Peng's group tuned the facet of TiO_2/Ti_3C_2 using a hydrothermal method without using an additional TiO_2 precursor (Fig. 7a, b) [71, 93]. $NaBF_4$ and NH_4F were used as reagents to, respectively, control morphology in the synthesis of (001) TiO_2/Ti_3C_2 and (111) TiO_2/Ti_3C_2, which were then applied in methyl orange degradation. Both the facet type of TiO_2 and the ratio of TiO_2 to Ti_3C_2 could be controlled by changing the duration of the hydrothermal reaction. Jia et al. [94] obtained closely aggregated TiO_2 nanorods with high carbon doping starting from Ti_3C_2 flakes and demonstrated a better photoactivity than commercially available P25 for hydrogen production (Fig. 7c). The carbon doping also changed the electron structure of TiO_2 and enhanced its light absorption ability. Peng et al. [95] also used Ti_3C_2 as a hole trap and Cu as an electron trap to separate the charges through a dual-carrier-separation mechanism, showing the potential of MXene as an efficient functional material for photocatalysis (Fig. 7d).

Calcination under atmosphere containing gases such as CO_2 and O_2 is another method used for the controlled oxidation of MXenes (Fig. 8). Lu et al. [96] obtained $Ti_3C_2/TiO_2/CuO$ by annealing $Cu(NO_3)_2$ and Ti_3C_2 together under argon atmosphere (Fig. 8a). Because of its good electronic conductivity, the incorporation of Ti_3C_2 improved electron/hole separation and led to better methyl orange degradation. Yuan et al. [97] annealed Ti_3C_2 in CO_2 to prepare 2D-layered C/TiO_2 hybrids used in hydrogen production, in which the presence of 2D carbon layers increased electron transport channels and enhanced charge separation efficiency (Fig. 8b). In addition, the effects of oxidation temperature

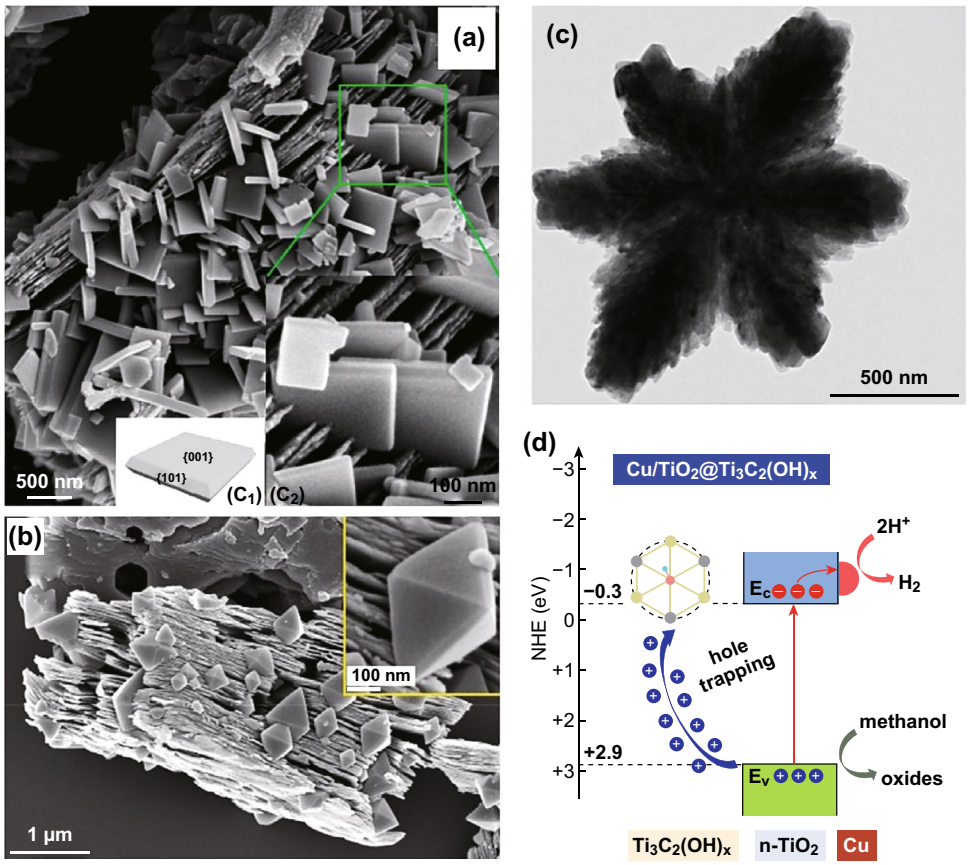

Fig. 7 In situ oxidized MXenes by hydrothermal method for photocatalysis. SEM images taken from **a** Peng et al. Reprinted with permission from Ref. [71]. Copyright 2016 American Chemical Society. **b** Peng et al. Reprinted with permission from Ref. [93]. Copyright 2017 Elsevier. **c** TEM image from Jia et al. Reprinted with permission from Ref. [94]. Copyright 2018 American Chemical Society. **d** Charge transfer in Cu/TiO_2@$Ti_3C_2(OH)_x$ from Peng et al. Reprinted with permission from Ref. [95]. Copyright 2018 Elsevier

and CO_2 on the grain size and crystal structure of TiO_2 were also investigated, revealing that increasing oxidation temperature and CO_2 gas flux led to larger grain sizes and more rutile TiO_2 formation. Low et al. [98] calcined Ti_3C_2 at different temperatures, enabling the in situ growth of TiO_2 nanoparticles on Ti_3C_2 nanosheets, thus forming TiO_2/Ti_3C_2 composites with different loading amounts of TiO_2 with the aim to improve performance in CO_2 reduction reaction (Fig. 8c). Interestingly, three main products were obtained during the photocatalytic CO_2 reduction process due to the sufficiently high intrinsic reduction potential of TiO_2. Results of the study also pointed out that excess of Ti_3C_2 in the composite could have an adverse effect on photocatalytic performance. Su et al. [99] used CO_2 to partially oxidize Nb_2C to form Nb_2O_5/Nb_2C composites for hydrogen production, where Nb_2O_5 and metallic Nb_2C served, respectively, as the semiconductor photocatalyst and co-catalyst (Fig. 8d). The easily formed junction at the interface served as an electron sink to efficiently capture photogenerated electrons and suppress recombination of photogenerated electron–hole pairs, thus enhancing the efficiency of charge separation and contributing to improved photocatalytic activity [71, 93, 99, 102].

Besides the hydrothermal method and calcination, other routes such as chemical oxidization and high-energy ball milling were also used to oxidize MXenes (Fig. 9). Cheng et al. [100] oxidized Ti_3C_2 flakes with 30% H_2O_2 to form microporous-MXene/TiO_{2-x} nanodots (Fig. 9a). This composite worked as a photo-Fenton bifunctional catalyst for Rhodamine B degradation under both dark and illumination conditions. Li et al. [101] synthesized TiO_2@C nanosheets from Ti_2C by high-energy ball milling and used it for methylene blue degradation (Fig. 9b). Shortly thereafter, our group used water to oxidize Ti_3C_2 to be applied in hydrogen

 https://doi.org/10.1007/s40820-019-0309-6

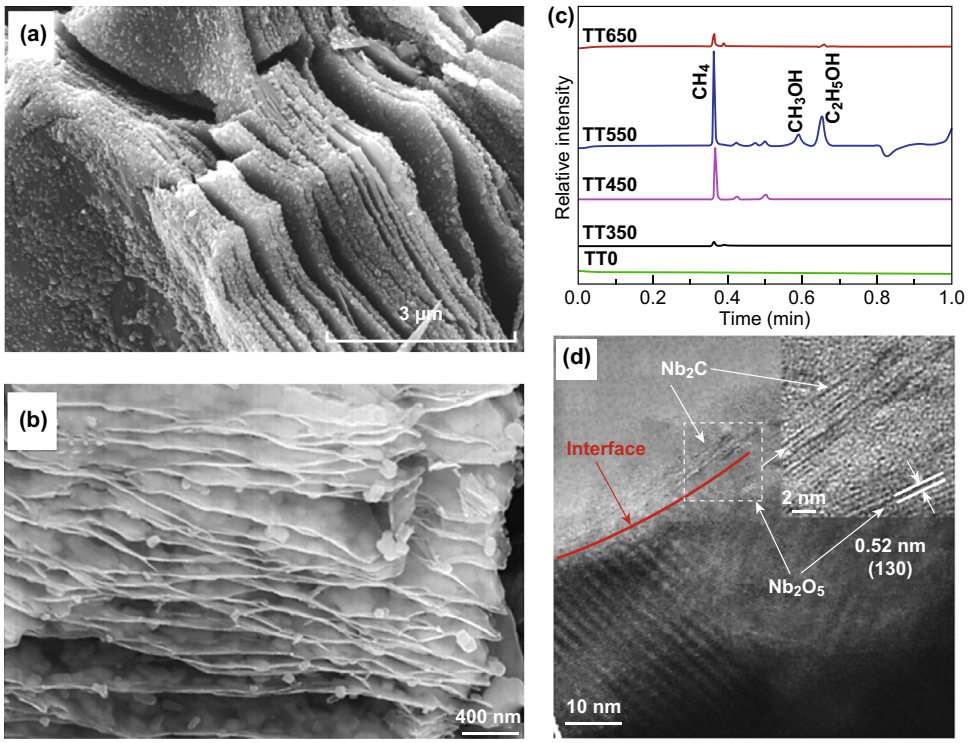

Fig. 8 Photocatalysts containing in situ oxidized MXenes formed by calcination. SEM images from **a** Lu et al. Reprinted with permission from Ref. [96]. Copyright 2017 Hindawi. **b** Yuan et al. Reprinted with permission from Ref. [97]. Copyright 2017 John Wiley & Sons. **c** Gaseous products of CO_2 reduction from Low et al. Reprinted with permission from Ref. [98]. Copyright 2018 Elsevier. **d** TEM image from Su et al. Reprinted with permission from Ref. [99]. Copyright 2018 John Wiley & Sons

production using Eosin Y as a sensitizer [102]. Similar to other oxidized MXenes, amorphous carbon and TiO_2 were formed after oxidation (Fig. 9c, d). The various MXene-derived composites obtained by in situ oxidation to be used as photocatalysts are listed in Table 1.

The MXenes oxidation is different from other methods because of the residual presence of carbon (mostly amorphous carbon) after oxidation, and the M element is oxidized into metal oxide on the carbon layer. Thus, the composite obtained is of the form metal oxide/MXenes/C. Both MXenes and C can be used as co-catalysts in the photocatalysis process. However, in this method, the ratio of the photocatalyst to MXenes varies within a certain range since no precursor is introduced. The limitation of this method is that only a few semiconductors (depending on M element) can be used as the photocatalyst.

3 Mechanism of MXenes as Co-catalysts

Since MXenes are conductors and serve as co-catalysts, the mechanism of action of a MXenes-based photocatalytic system is through accelerated charge separation and suppression of carrier recombination [69–71]. The photocatalysts absorb visible light and photogenerated electrons are excited to the CB, while holes are left in the valence band (VB). The excited charge carriers are transferred to MXenes at the interface mainly because of the higher potential of MXenes. Electrons transfer to MXenes without recombination and react on the MXene surface to generate H_2 by reducing H^+ [74, 78, 81, 91, 94, 102, 103], CH_4 and CO by reducing CO_2 [88, 98], or NH_3 by reducing N_2 [19], as shown in Fig. 10 process (a). In process (b), holes transfer to MXenes and react to produce OH· that can be utilized for degradation of organics [71, 93, 95]; electrons can also produce OH· for organic degradation [71, 93]. The charge transfer process

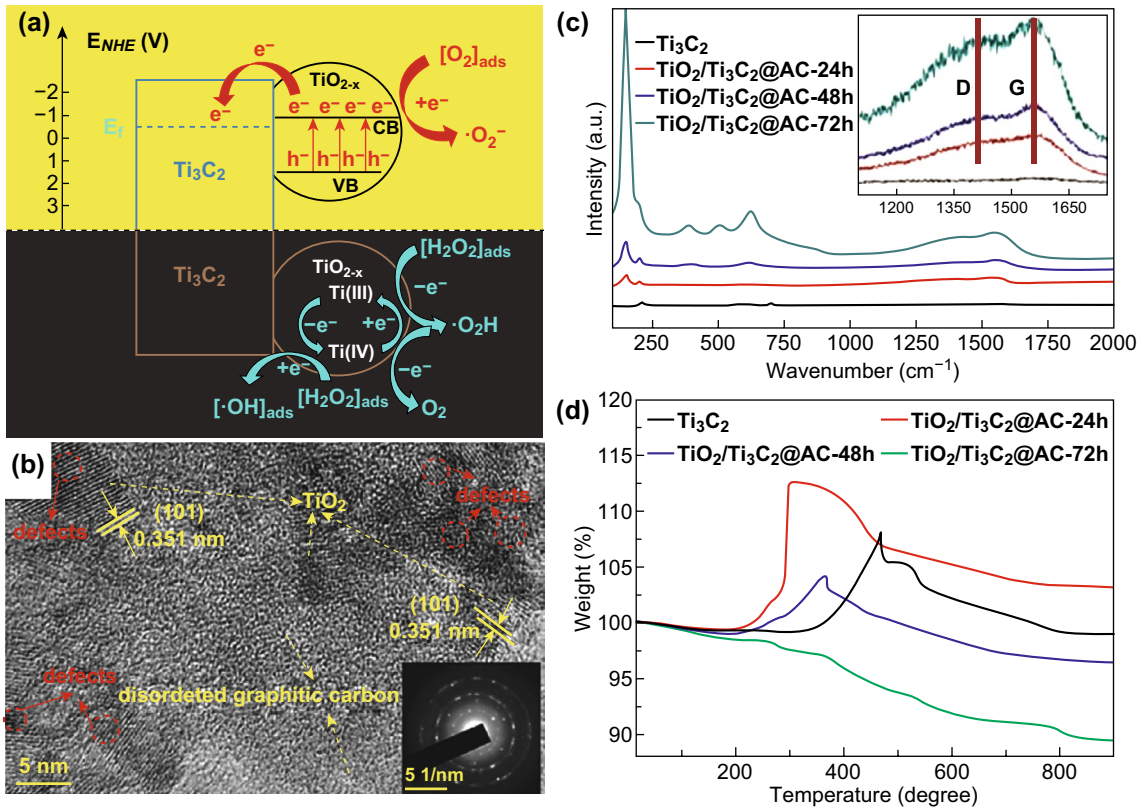

Fig. 9 MXene-derived photocatalysts synthesized by other in situ oxidation methods. **a** Mechanisms of degradation over mp-MXene/TiO_{2-x} from Cheng et al. Reprinted with permission from Ref. [100]. Copyright 2018 The Royal Society of Chemistry. **b** TEM image from Li et al. Reprinted with permission from Ref. [101]. Copyright 2018 Elsevier. **c** Raman spectra and **d** TGA from Sun et al. Reprinted with permission from Ref. [102]. Copyright 2018 The Royal Society of Chemistry

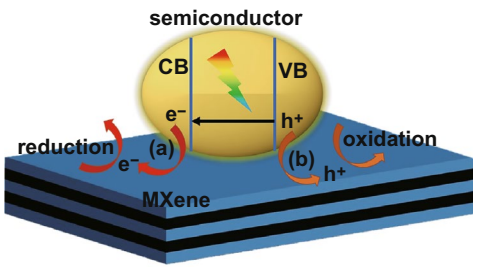

Fig. 10 Schematic of the working mechanism of MXenes applied in photocatalysis

from the photocatalyst to MXenes improves electron–hole pair separation and suppresses charge recombination in photocatalysts, thus enhancing the photoactivity.

Another advantage of using MXenes in photocatalysis is due to their termination groups. For example, –O termination groups show the best potential for hydrogen production because of their low $|\Delta G_H|$ and the availability of active sites for the adsorption of hydrogen atoms [70, 74]. Though termination groups are important in photocatalysis, currently, it has not been possible to precisely control the relative concentrations of the different termination groups. Using presently available synthetic methods, changing the different reaction conditions can partially modify the termination groups on MXenes surface and thereby affect their performance in photocatalysis.

4 Conclusion and Outlook

In summary, the application of MXenes in photocatalysis has shown rapid development since 2015. Among the MXenes family, Ti_3C_2 has been the most studied MXene. Mechanical mixing and self-assembly are mild and easy methods of synthesis, where the ratio of MXenes to the photocatalyst can be controlled. In addition, MXenes can also be doped into the photocatalysts by in situ decoration of a semiconductor photocatalyst. The large interfacial area afforded by

https://doi.org/10.1007/s40820-019-0309-6

the doping process improves electron transfer. However, the MXenes oxidation method has the advantage of obtaining both carbon and MXenes as co-catalysts by forming a metal oxide/MXenes/C structure. Though the above-mentioned four synthetic methods are generally used for photocatalysts, with further development in the field of MXenes, new processes may be discovered.

Besides developing improved synthetic methods, the other aspects that need to be focused on in the future are as follows:

1. Controlling the morphologies of MXenes. MXene flakes show larger surface area than multilayered MXenes, since mono- or few-layered MXenes provide a greater number of active sites for photocatalytic reactions. The flakes are also convenient for building structures, such as quantum dots, spheres, and nanorods. However, the instability of MXenes should be taken into account during heat treatment [107].
2. MXenes combine with efficient photocatalysts. MXenes can be used as co-catalysts to combine with many semiconductor photocatalysts due to their excellent electronic conductivity and the presence of numerous hydrophilic groups on the surface. Hundreds of semiconductor photocatalysts have been reported for photocatalysis so far. Attention should be paid to combining the efficient and cheap photocatalysts with MXenes to achieve better photocatalytic performance. So far, only g-C_3N_4, CdS, ZnS, TiO_2, CuO, Nb_2O_5, $BiVO_4$, Ag_3PO_4, α-Fe_2O_3, In_2S_3, Bi_2WO_6, $Bi_{0.90}Gd_{0.10}Fe_{0.80}Sn_{0.20}O_3$, and BiOBr have been explored, with TiO_2 and g-C_3N_4 attracting the most attention.
3. Surface modification of MXenes. Surface termination groups significantly affect the properties of MXenes, and thus, tuning the surface termination groups and modifying the MXenes surface are expected to greatly influence its potential as co-catalyst.
4. Synthesis of new MXenes. To date, only a small fraction of the different possible MXenes has been synthesized in laboratories. Some MXenes showing semiconducting properties have been reported based on theoretical calculations. Theoretical predictions help in the synthesis of semiconductor MXenes and applied in photocatalysis. Once obtained experimentally, potential MXenes can be applied as photocatalysts, thus widening the application range of MXenes. Moreover, new types of transition metal borides (MBenes) have also been predicted [34, 109] and have shown potential for photocatalysis applications. More work needs to be done in this direction.
5. Developing new synthesis methods for MXenes. HF and in situ HF wet chemical treatment are by far the most used methods in MXenes synthesis. Other HF-free methods are emerging and leading to MXenes with different properties. Yet, these have not been investigated in photocatalytic applications, and thus, the effect of the type of synthesis process used on the final performance of the MXene is currently not understood.

In short, due to tremendous effort of scientists worldwide, the great potential of MXenes in photocatalysis has been revealed. With the fast-growing development in this area, it is expected that more and more studies will focus on the applications of MXenes photocatalysis and pave the way to the commercialization of photocatalytic technologies based on these materials.

Acknowledgements This work was supported by the National Natural Science Foundation of China (No. 11574111 and No. 11974129 to X.-F. W.) and "the Fundamental Research Funds for the Central Universities."

References

1. M. Naguib, M. Kurtoglu, V. Presser, J. Lu, J. Niu et al., Two-dimensional nanocrystals produced by exfoliation of Ti_3AlC_2. Adv. Mater. **23**, 4248–4253 (2011). https://doi.org/10.1002/adma.201102306
2. M. Naguib, V.N. Mochalin, M.W. Barsoum, Y. Gogotsi, 25th anniversary article: MXenes: a new family of two-dimensional materials. Adv. Mater. **26**, 992–1005 (2014). https://doi.org/10.1002/adma.201304138
3. B. Anasori, M.R. Lukatskaya, Y. Gogotsi, 2D metal carbides and nitrides (MXenes) for energy storage. Nat. Rev. Mater. **2**, 16098 (2017). https://doi.org/10.1038/natrevmats.2016.98
4. M. Liu, Z. Yang, H. Sun, C. Lai, X. Zhao, H. Peng, T. Liu, A hybrid carbon aerogel with both aligned and interconnected pores as interlayer for high-performance lithium–sulfur batteries. Nano Res. **9**, 3735–3746 (2016). https://doi.org/10.1007/s12274-016-1244-1
5. C. Hou, Z. Tai, L. Zhao, Y. Zhai, Y. Hou et al., High performance MnO@C microcages with a hierarchical structure and tunable carbon shell for efficient and durable lithium

storage. J. Mater. Chem. A **6**, 9723–9736 (2018). https://doi.org/10.1039/c8ta02863j

6. B. Kirubasankar, V. Murugadoss, J. Lin, T. Ding, M. Dong et al., In situ grown nickel selenide on graphene nanohybrid electrodes for high energy density asymmetric supercapacitors. Nanoscale **10**, 20414–20425 (2018). https://doi.org/10.1039/c8nr06345a
7. M. Liu, Q. Meng, Z. Yang, X. Zhao, T. Liu, Ultra-long-term cycling stability of an integrated carbon-sulfur membrane with dual shuttle-inhibiting layers of graphene "nets" and a porous carbon skin. Chem. Commun. **54**, 5090–5093 (2018). https://doi.org/10.1039/c8cc01889h
8. W. Du, X. Wang, J. Zhan, X. Sun, L. Kang et al., Biological cell template synthesis of nitrogen-doped porous hollow carbon spheres/MnO_2 composites for high-performance asymmetric supercapacitors. Electrochim. Acta **296**, 907–915 (2019). https://doi.org/10.1016/j.electacta.2018.11.074
9. C. Hou, J. Wang, W. Du, J. Wang, Y. Du et al., One-pot synthesized molybdenum dioxide–molybdenum carbide heterostructures coupled with 3D holey carbon nanosheets for highly efficient and ultrastable cycling lithium-ion storage. J. Mater. Chem. A **7**, 13460–13472 (2019). https://doi.org/10.1039/c9ta03551f
10. M. Idrees, S. Batool, J. Kong, Q. Zhuang, H. Liu et al., Polyborosilazane derived ceramics-nitrogen sulfur dual doped graphene nanocomposite anode for enhanced lithium ion batteries. Electrochim. Acta **296**, 925–937 (2019). https://doi.org/10.1016/j.electacta.2018.11.088
11. K. Le, Z. Wang, F. Wang, Q. Wang, Q. Shao et al., Sandwich-like NiCo layered double hydroxide/reduced graphene oxide nanocomposite cathodes for high energy density asymmetric supercapacitors. Dalton Trans. **48**, 5193–5202 (2019). https://doi.org/10.1039/c9dt00615j
12. R. Li, X. Zhu, Q. Fu, G. Liang, Y. Chen et al., Nanosheet-based $Nb_{12}O_{29}$ hierarchical microspheres for enhanced lithium storage. Chem. Commun. **55**, 2493–2496 (2019). https://doi.org/10.1039/c8cc09924c
13. Y. Ma, C. Hou, H. Zhang, Q. Zhang, H. Liu, S. Wu, Z. Guo, Three-dimensional core-shell Fe_3O_4/polyaniline coaxial heterogeneous nanonets: Preparation and high performance supercapacitor electrodes. Electrochim. Acta **315**, 114–123 (2019). https://doi.org/10.1016/j.electacta.2019.05.073
14. L. Yang, M. Shi, J. Jiang, Y. Liu, C. Yan, H. Liu, Z. Guo, Heterogeneous interface induced formation of balsam pear-like ppy for high performance supercapacitors. Electrochim. Acta **244**, 27–30 (2019). https://doi.org/10.1016/j.matlet.2019.02.064
15. M. Liu, Y. Liu, Y. Yan, F. Wang, J. Liu, T. Liu, A highly conductive carbon–sulfur film with interconnected mesopores as an advanced cathode for lithium-sulfur batteries. Chem. Commun. **53**, 9097–9100 (2017). https://doi.org/10.1039/c7cc04523a
16. T. Hisatomi, K. Domen, Introductory lecture: sunlight-driven water splitting and carbon dioxide reduction by heterogeneous semiconductor systems as key processes in artificial photosynthesis. Faraday Discuss. **198**, 11–35 (2017). https://doi.org/10.1039/c6fd00221h
17. V.-H. Nguyen, J.C.S. Wu, Recent developments in the design of photoreactors for solar energy conversion from water splitting and CO_2 reduction. Appl. Cataly. A Gen. **550**, 122–141 (2018). https://doi.org/10.1016/j.apcata.2017.11.002
18. X. Zhang, Z. Zhang, J. Li, X. Zhao, D. Wu, Z. Zhou, Ti_2CO_2 MXene: a highly active and selective photocatalyst for CO_2 reduction. J. Mater. Chem. A **5**, 12899–12903 (2017). https://doi.org/10.1039/c7ta03557h
19. Q. Liu, L. Ai, J. Jiang, MXene-derived TiO_2@C/g-C_3N_4 heterojunctions for highly efficient nitrogen photofixation. J. Mater. Chem. A **6**, 4102–4110 (2018). https://doi.org/10.1039/c7ta09350k
20. J. Low, J. Yu, M. Jaroniec, S. Wageh, A.A. Al-Ghamdi, Heterojunction photocatalysts. Adv. Mater. **29**, 1601694–1601713 (2017). https://doi.org/10.1002/adma.201601694
21. D. Pan, S. Ge, J. Zhao, Q. Shao, L. Guo, X. Zhang, J. Lin, G. Xu, Z. Guo, Synthesis, characterization and photocatalytic activity of mixed-metal oxides derived from NiCoFe ternary layered double hydroxides. Dalton Trans. **47**, 9765–9778 (2018). https://doi.org/10.1039/c8dt01045e
22. J. Zhao, S. Ge, D. Pan, Q. Shao, J. Lin et al., Solvothermal synthesis, characterization and photocatalytic property of zirconium dioxide doped titanium dioxide spinous hollow microspheres with sunflower pollen as bio-templates. J. Colloid Interface Sci. **529**, 111–121 (2018). https://doi.org/10.1016/j.jcis.2018.05.091
23. Y. Sheng, J. Yang, F. Wang, L. Liu, H. Liu, C. Yan, Z. Guo, Sol-gel synthesized hexagonal boron nitride/titania nanocomposites with enhanced photocatalytic activity. Appl. Surf. Sci. **465**, 154–163 (2019). https://doi.org/10.1016/j.apsusc.2018.09.137
24. J. Tian, Q. Shao, J. Zhao, D. Pan, M. Dong et al., Microwave solvothermal carboxymethyl chitosan templated synthesis of TiO_2/ZrO_2 composites toward enhanced photocatalytic degradation of Rhodamine B. J. Colloid Interface Sci. **541**, 18–29 (2019). https://doi.org/10.1016/j.jcis.2019.01.069
25. J. Zhao, S. Ge, D. Pan, Y. Pan, V. Murugadoss et al., Microwave hydrothermal synthesis of In_2O_3-ZnO nanocomposites and their enhanced photoelectrochemical properties. J. Electrochem. Soc. **166**, H3074–H3083 (2019). https://doi.org/10.1149/2.0071905jes
26. H. Shindume, L.Z. Zhao, N. Wang, H. Liu, A. Umar, J. Zhang, T. Wu, Z. Guo, Enhanced photocatalytic activity of B, N-codoped TiO_2 by a new molten nitrate process. Electrochim. Acta **19**, 839–849 (2019). https://doi.org/10.1166/jnn.2019.15745
27. Z. Zhao, H. An, J. Lin, M. Feng, V. Murugadoss et al., Progress on the photocatalytic reduction removal of chromium contamination. Chem. Rec. **19**, 873–882 (2019). https://doi.org/10.1002/tcr.201800153
28. G. Zheng, J. Wang, H. Liu, V. Murugadoss, G. Zu et al., Tungsten oxide nanostructures and nanocomposites for photoelectrochemical water splitting. Nanoscale (advance Article, 2019). https://doi.org/10.1039/c9nr03474a

 https://doi.org/10.1007/s40820-019-0309-6

29. B. Lin, Z. Lin, S. Chen, M. Yu, W. Li et al., Surface intercalated spherical $MoS_{2x}Se_{2(1-x)}$ nanocatalysts for highly efficient and durable hydrogen evolution reactions. Dalton Trans. **48**, 8279–8287 (2019). https://doi.org/10.1039/c9dt01218d
30. T. Su, Q. Shao, Z. Qin, Z. Guo, Z. Wu, Role of interfaces in two-dimensional photocatalyst for water splitting. ACS Catal. **8**, 2253–2276 (2018). https://doi.org/10.1021/acscatal.7b03437
31. M. Ge, J. Cai, J. Iocozzia, C. Cao, J. Huang et al., A review of TiO_2 nanostructured catalysts for sustainable H_2 generation. Int. J. Hydrog. Energy **42**, 8418–8449 (2017). https://doi.org/10.1016/j.ijhydene.2016.12.052
32. L. Clarizia, D. Russo, I. Di Somma, R. Andreozzi, R. Marotta, Hydrogen generation through solar photocatalytic processes: a review of the configuration and the properties of effective metal-based semiconductor nanomaterials. Energies **10**, 1624–1644 (2017). https://doi.org/10.3390/en10101624
33. X. Zhang, Z. Zhang, Z. Zhou, MXene-based materials for electrochemical energy storage. J. Energy Chem. **27**, 73–85 (2018). https://doi.org/10.1016/j.jechem.2017.08.004
34. Z. Guo, J. Zhou, Z. Sun, New two-dimensional transition metal borides for Li ion batteries and electrocatalysis. J. Mater. Chem. A **5**, 23530–23535 (2017). https://doi.org/10.1039/c7ta08665b
35. H. Jiang, Z. Wang, Q. Yang, L. Tan, L. Dong, M. Dong, Ultrathin Ti_3C_2T (MXene) nanosheet-wrapped $NiSe_2$ octahedral crystal for enhanced supercapacitor performance and synergetic electrocatalytic water splitting. Nano-Micro Lett. **11**, 31 (2019). https://doi.org/10.1007/s40820-019-0261-5
36. Y.T. Liu, P. Zhang, N. Sun, B. Anasori, Q.Z. Zhu, H. Liu, Y. Gogotsi, B. Xu, Self-assembly of transition metal oxide nanostructures on MXene nanosheets for fast and stable lithium storage. Adv. Mater. **30**, 1707334 (2018). https://doi.org/10.1002/adma.201707334
37. L. Yu, L. Hu, B. Anasori, Y.-T. Liu, Q. Zhu, P. Zhang, Y. Gogotsi, B. Xu, MXene-bonded activated carbon as a flexible electrode for high-performance supercapacitors. ACS Energy Lett. **3**, 1597–1603 (2018). https://doi.org/10.1021/acsenergylett.8b00718
38. H. Liu, X. Zhang, Y. Zhu, B. Cao, Q. Zhu et al., Electrostatic self-assembly of 0D-2D SnO_2 quantum dots/$Ti_3C_2T_x$ MXene hybrids as anode for lithium-ion batteries. Nano-Micro Lett. **11**, 65 (2019). https://doi.org/10.1007/s40820-019-0296-7
39. F. Shahzad, M. Alhabeb, C.B. Hatter, B. Anasori, H.S. Man, C.M. Koo, Y. Gogotsi, Electromagnetic interference shielding with 2D transition metal carbides (MXenes). Science **353**, 1137 (2016). https://doi.org/10.1126/science.aag2421
40. M. Han, X. Yin, X. Li, B. Anasori, L. Zhang, L. Cheng, Y. Gogotsi, Laminated and two-dimensional carbon-supported microwave absorbers derived from MXenes. ACS Appl. Mater. Interfaces **9**, 20038–20045 (2017). https://doi.org/10.1021/acsami.7b04602
41. J. Zhu, E. Ha, G. Zhao, Y. Zhou, D. Huang et al., Recent advance in MXenes: a promising 2D material for catalysis, sensor and chemical adsorption. Coord. Chem. Rev. **352**, 306–327 (2017). https://doi.org/10.1016/j.ccr.2017.09.012
42. A. Sarycheva, A. Polemi, Y. Liu, K. Dandekar, B. Anasori, Y. Gogotsi, 2D titanium carbide (MXene) for wireless communication. Sci. Adv. **4**, eaau0920 (2018). https://doi.org/10.1126/sciadv.aau0920
43. Y. Ying, Y. Liu, X. Wang, Y. Mao, W. Cao, P. Hu, X. Peng, Two-dimensional titanium carbide for efficiently reductive removal of highly toxic chromium(VI) from water. ACS Appl. Mater. Interfaces **7**, 1795–1803 (2015). https://doi.org/10.1021/am5074722
44. N. Liu, N. Lu, Y. Su, P. Wang, X. Quan, Fabrication of g-C_3N_4/Ti_3C_2 composite and its visible-light photocatalytic capability for ciprofloxacin degradation. Sep. Purif. Technol. **211**, 782–789 (2019). https://doi.org/10.1016/j.seppur.2018.10.027
45. C. Dall'Agnese, Y. Dall'Agnese, B. Anasori, W. Sugimoto, S. Mori, Oxidized Ti_3C_2 MXene nanosheets for dye-sensitized solar cells. New J. Chem. **42**, 16446–16450 (2018). https://doi.org/10.1039/c8nj03246g
46. L. Yang, Y. Dall'Agnese, K. Hantanasirisakul, C.E. Shuck, K. Maleski et al., SnO_2–Ti_3C_2 MXene electron transport layers for perovskite solar cells. J. Mater. Chem. A **7**, 5635–5642 (2019). https://doi.org/10.1039/c8ta12140k
47. H.C. Fu, V. Ramalingam, H. Kim, C.H. Lin, X. Fang, H.N. Alshareef, J.H. He, MXene-contacted silicon solar cells with 11.5% efficiency. Adv. Energy Mater. (2019). https://doi.org/10.1002/aenm.201900180
48. H. Wang, Y. Wu, X. Yuan, G. Zeng, J. Zhou, X. Wang, J.W. Chew, Clay-inspired MXene-based electrochemical devices and photo-electrocatalyst: state-of-the-art progresses and challenges. Adv. Mater. **30**, 1704561 (2018). https://doi.org/10.1002/adma.201704561
49. M. Li, J. Lu, K. Luo, Y. Li, K. Chang et al., Element replacement approach by reaction with lewis acidic molten salts to synthesize nanolaminated MAX phases and MXenes. J. Am. Chem. Soc. **141**, 4730–4737 (2019). https://doi.org/10.1021/jacs.9b00574
50. X. Lu, K. Xu, P. Chen, K. Jia, S. Liu, C. Wu, Facile one step method realizing scalable production of g-c_3n_4 nanosheets and study of their photocatalytic H_2 evolution activity. J. Mater. Chem. A **2**, 18924–18928 (2014). https://doi.org/10.1039/c4ta04487h
51. J. Peng, X. Chen, W.-J. Ong, X. Zhao, N. Li, Surface and heterointerface engineering of 2D MXenes and their nanocomposites: insights into electro- and photocatalysis. Chem **5**, 18–50 (2019). https://doi.org/10.1016/j.chempr.2018.08.037
52. Z.W. Seh, K.D. Fredrickson, B. Anasori, J. Kibsgaard, A.L. Strickler et al., Two-dimensional molybdenum carbide (MXene) as an efficient electrocatalyst for hydrogen evolution. ACS Energy Lett. **1**, 589–594 (2016). https://doi.org/10.1021/acsenergylett.6b00247
53. M. Alhabeb, K. Maleski, T.S. Mathis, A. Sarycheva, C.B. Hatter, S. Uzun, A. Levitt, Y. Gogotsi, Selective etching of silicon from Ti_3SiC_2 (MAX) to obtain 2D titanium carbide (MXene). Angew. Chem. Int. Ed. **57**, 5444–5448 (2018). https://doi.org/10.1002/anie.201802232

54. J. Xuan, Z. Wang, Y. Chen, D. Liang, L. Cheng et al., Organic-base-driven intercalation and delamination for the production of functionalized titanium carbide nanosheets with superior photothermal therapeutic performance. Angew. Chem. Int. Ed. **128**, 14789–14794 (2016). https://doi.org/10.1002/ange.201606643
55. S. Yang, P. Zhang, F. Wang, A.G. Ricciardulli, M.R. Lohe, P.W.M. Blom, X. Feng, Fluoride-free synthesis of two-dimensional titanium carbide (MXene) using a binary aqueous system. Angew. Chem. Int. Ed. **57**, 15491–15495 (2018). https://doi.org/10.1002/anie.201809662
56. M.R. Lukatskaya, J. Halim, B. Dyatkin, M. Naguib, Y.S. Buranova et al., Room-temperature carbide-derived carbon synthesis by electrochemical etching of MAX phases. Angew. Chem. Int. Ed. **53**, 4877–4880 (2014). https://doi.org/10.1002/anie.201402513
57. S.Y. Pang, Y.T. Wong, S. Yuan, Y. Liu, M.K. Tsang et al., Universal strategy for HF-free facile and rapid synthesis of two-dimensional MXenes as multifunctional energy materials. J. Am. Chem. Soc. **141**(24), 9610–9616 (2019). https://doi.org/10.1021/jacs.9b02578
58. T. Li, L. Yao, Q. Liu, J. Gu, R. Luo et al., Fluorine-free synthesis of high-purity $Ti_3C_2T_x$ (T = OH, O) via alkali treatment. Angew. Chem. Int. Ed. **57**, 6115–6119 (2018). https://doi.org/10.1002/anie.201800887
59. M. Alhabeb, K. Maleski, B. Anasori, P. Lelyukh, L. Clark, S. Sin, Y. Gogotsi, Guidelines for synthesis and processing of two-dimensional titanium carbide ($Ti_3C_2T_x$ MXene). Chem. Mater. **29**, 7633–7644 (2017). https://doi.org/10.1021/acs.chemmater.7b02847
60. X. Xiao, H. Wang, P. Urbankowski, Y. Gogotsi, Topochemical synthesis of 2D materials. Chem. Soc. Rev. **47**, 8744–8765 (2018). https://doi.org/10.1039/c8cs00649k
61. V.M. Ng, H. Huang, K. Zhou, P.S. Lee, W. Que, J.Z. Xu, L.B. Kong, Recent progress in layered transition metal carbides and/or nitrides (MXenes) and their composites: synthesis and applications. J. Mater. Chem. A **5**(7), 3039–3068 (2017). https://doi.org/10.1039/c6ta06772g
62. J. Pang, R.G. Mendes, A. Bachmatiuk, L. Zhao, H.Q. Ta et al., Applications of 2D MXenes in energy conversion and storage systems. Chem. Soc. Rev. **48**, 72–133 (2019). https://doi.org/10.1039/c8cs00324f
63. Z. Guo, J. Zhou, L. Zhu, Z. Sun, MXene: a promising photocatalyst for water splitting. J. Mater. Chem. A **4**, 11446–11452 (2016). https://doi.org/10.1039/c6ta04414j
64. S.-Y. Xie, J.-H. Su, H. Zheng, Group-IV analogues of MXene: promising two-dimensional semiconductors. Solid State Commun. **291**, 51–53 (2019). https://doi.org/10.1016/j.ssc.2019.01.017
65. C.-F. Fu, X. Li, Q. Luo, J. Yang, Two-dimensional multilayer M_2CO_2 (M = Sc, Zr, Hf) as photocatalysts for hydrogen production from water splitting: a first principles study. J. Mater. Chem. A **5**, 24972–24980 (2017). https://doi.org/10.1039/c7ta08812d
66. Z. Guo, N. Miao, J. Zhou, B. Sa, Z. Sun, Strain-mediated type-I/type-II transition in MXene/blue phosphorene van der Waals heterostructures for flexible optical/electronic devices. J. Mater. Chem. C **5**, 978–984 (2017). https://doi.org/10.1039/c6tc04349f
67. J. Cui, Q. Peng, J. Zhou, Z. Sun, Strain-tunable electronic structures and optical properties of semiconducting MXenes. Nanotechnology **30**, 345205 (2019). https://doi.org/10.1088/1361-6528/ab1f22
68. A. Mostafaei, E. Faizabadi, E.H. Semiromi, Theoretical studies and tuning the electronic and optical properties of Zr_2CO_2 monolayer using biaxial strain effect: modified Becke–Johnson calculation. Physica E **114**, 113559 (2019). https://doi.org/10.1016/j.physe.2019.113559
69. M. Ye, X. Wang, E. Liu, J. Ye, D. Wang, Boosting the photocatalytic activity of P25 for carbon dioxide reduction by using a surface-alkalinized titanium carbide MXene as cocatalyst. Chemsuschem **11**, 1606–1611 (2018). https://doi.org/10.1002/cssc.201800083
70. J. Ran, G. Gao, F.T. Li, T.Y. Ma, A. Du, S.Z. Qiao, Ti_3C_2 MXene co-catalyst on metal sulfide photo-absorbers for enhanced visible-light photocatalytic hydrogen production. Nat. Commun. **8**, 13907 (2017). https://doi.org/10.1038/ncomms13907
71. C. Peng, X. Yang, Y. Li, H. Yu, H. Wang, F. Peng, Hybrids of two-dimensional Ti_3C_2 and TiO_2 exposing 001 facets toward enhanced photocatalytic activity. ACS Appl. Mater. Interfaces **8**, 6051–6060 (2016). https://doi.org/10.1021/acsami.5b11973
72. X. An, W. Wang, J. Wang, H. Duan, J. Shi, X. Yu, The synergetic effects of Ti_3C_2 MXene and Pt as co-catalysts for highly efficient photocatalytic hydrogen evolution over g-C_3N_4. Phys. Chem. Chem. Phys. **20**, 11405–11411 (2018). https://doi.org/10.1039/c8cp01123k
73. X. Xie, N. Zhang, Z.-R. Tang, M. Anpo, Y.-J. Xu, $Ti_3C_2T_x$ MXene as a Janus cocatalyst for concurrent promoted photoactivity and inhibited photocorrosion. Appl. Catal. B **237**, 43–49 (2018). https://doi.org/10.1016/j.apcatb.2018.05.070
74. Y. Sun, D. Jin, Y. Sun, X. Meng, Y. Gao et al., G-C_3N_4/$Ti_3C_2T_x$ (MXenes) composite with oxidized surface groups for efficient photocatalytic hydrogen evolution. J. Mater. Chem. A **6**, 9124–9131 (2018). https://doi.org/10.1039/c8ta02706d
75. T. Cai, L. Wang, Y. Liu, S. Zhang, W. Dong et al., Ag_3PO_4/Ti_3C_2 MXene interface materials as a Schottky catalyst with enhanced photocatalytic activities and anti-photocorrosion performance. Appl. Catal. B **239**, 545–554 (2018). https://doi.org/10.1016/j.apcatb.2018.08.053
76. H. Zhang, M. Li, J. Cao, Q. Tang, P. Kang, C. Zhu, M. Ma, 2D a-Fe_2O_3 doped Ti_3C_2 MXene composite with enhanced visible light photocatalytic activity for degradation of Rhodamine B. Ceram. Int. **44**, 19958–19962 (2018). https://doi.org/10.1016/j.ceramint.2018.07.262
77. T. Su, Z.D. Hood, M. Naguib, L. Bai, S. Luo et al., Monolayer $Ti_3C_2T_x$ as an effective co-catalyst for enhanced photocatalytic hydrogen production over TiO_2. ACS Appl. Energy Mater. **2**, 4640–4651 (2019). https://doi.org/10.1021/acsaem.8b02268

 https://doi.org/10.1007/s40820-019-0309-6

78. T. Su, Z.D. Hood, M. Naguib, L. Bai, S. Luo et al., 2D/2D heterojunction of Ti_3C_2/g-C_3N_4 nanosheets for enhanced photocatalytic hydrogen evolution. Nanoscale **11**, 8138–8149 (2019). https://doi.org/10.1039/c9nr00168a
79. J.-H. Zhao, L.-W. Liu, K. Li, T. Li, F.-T. Liu, Conductive Ti_3C_2 and MOF-derived CoS_x boosting the photocatalytic hydrogen production activity of TiO_2. CrystEngComm **21**, 2416–2421 (2019). https://doi.org/10.1039/c8ce02050g
80. R. Chen, P. Wang, J. Chen, C. Wang, Y. Ao, Synergetic effect of MoS_2 and MXene on the enhanced H_2 evolution performance of CdS under visible light irradiation. Appl. Surf. Sci. **473**, 11–19 (2019). https://doi.org/10.1016/j.apsusc.2018.12.071
81. M. Shao, Y. Shao, J. Chai, Y. Qu, M. Yang et al., Synergistic effect of 2D Ti_2C and g-C_3N_4 for efficient photocatalytic hydrogen production. J. Mater. Chem. A **5**, 16748–16756 (2017). https://doi.org/10.1039/c7ta04122e
82. Y. Xu, S. Wang, J. Yang, B. Han, R. Nie et al., Highly efficient photoelectrocatalytic reduction of CO_2 on the Ti_3C_2/g-C_3N_4 heterojunction with rich Ti^{3+} and pyri-N species. J. Mater. Chem. A **6**, 15213–15220 (2018). https://doi.org/10.1039/c8ta03315c
83. Y. Gao, L. Wang, A. Zhou, Z. Li, J. Chen, H. Bala, Q. Hu, X. Cao, Hydrothermal synthesis of TiO_2/Ti_3C_2 nanocomposites with enhanced photocatalytic activity. Mater. Lett. **150**, 62–64 (2015). https://doi.org/10.1016/j.matlet.2015.02.135
84. H. Wang, R. Peng, Z.D. Hood, M. Naguib, S.P. Adhikari, Z. Wu, Titania composites with 2D transition metal carbides as photocatalysts for hydrogen production under visible-light irradiation. Chemsuschem **9**, 1490–1497 (2016). https://doi.org/10.1002/cssc.201600165
85. L. Shi, C. Xu, D. Jiang, X. Sun, X. Wang et al., Enhanced interaction in TiO_2/$BiVO_4$ heterostructures via MXene Ti_3C_2-derived 2D-carbon for highly efficient visible-light photocatalysis. Nanotechnology **30**, 075601 (2019). https://doi.org/10.1088/1361-6528/aaf313
86. Q. Luo, B. Chai, M. Xu, Q. Cai, Preparation and photocatalytic activity of TiO_2-loaded Ti_3C_2 with small interlayer spacing. Appl. Phys. A **124**, 495 (2018). https://doi.org/10.1007/s00339-018-1909-6
87. C. Liu, Q. Xu, Q. Zhang, Y. Zhu, M. Ji et al., Layered BiOBr/Ti_3C_2 MXene composite with improved visible-light photocatalytic activity. J. Mater. Sci. **54**, 2458–2471 (2018). https://doi.org/10.1007/s10853-018-2990-0
88. S. Cao, B. Shen, T. Tong, J. Fu, J. Yu, 2D/2D heterojunction of ultrathin MXene/Bi_2WO_6 nanosheets for improved photocatalytic CO_2 reduction. Adv. Funct. Mater. **28**, 1800136 (2018). https://doi.org/10.1002/adfm.201800136
89. A. Tariq, S.I. Ali, D. Akinwande, S. Rizwan, Efficient visible-light photocatalysis of 2D-MXene nanohybrids with Gd^{3+}- and Sn^{4+}-codoped bismuth ferrite. ACS Omega **3**, 13828–13836 (2018). https://doi.org/10.1021/acsomega.8b01951
90. H. Wang, Y. Wu, T. Xiao, X. Yuan, G. Zeng et al., Formation of quasi-core-shell In_2S_3/anatase TiO_2 @metallic $Ti_3C_2T_x$ hybrids with favorable charge transfer channels for excellent visible-light-photocatalytic performance. Appl. Catalysis B **233**, 213–225 (2018). https://doi.org/10.1016/j.apcatb.2018.04.012
91. L. Tie, S. Yang, C. Yu, H. Chen, Y. Liu, S. Dong, J. Sun, J. Sun, In situ decoration of ZnS nanoparticles with Ti_3C_2 MXene nanosheets for efficient photocatalytic hydrogen evolution. J. Colloid Interface Sci. **545**, 63–70 (2019). https://doi.org/10.1016/j.jcis.2019.03.014
92. T. Wojciechowski, A. Rozmyslowska-Wojciechowska, G. Matyszczak, M. Wrzecionek, A. Olszyna et al., Ti_2C MXene modified with ceramic oxide and noble metal nanoparticles: synthesis, morphostructural properties, and high photocatalytic activity. Inorg. Chem. **58**, 7602–7614 (2019). https://doi.org/10.1021/acs.inorgchem.9b01015
93. C. Peng, H. Wang, H. Yu, F. Peng, (111) TiO_{2-x}/Ti_3C_2: Synergy of active facets, interfacial charge transfer and Ti^{3+} doping for enhance photocatalytic activity. Mater. Res. Bull. **89**, 16–25 (2017). https://doi.org/10.1016/j.materresbull.2016.12.049
94. G. Jia, Y. Wang, X. Cui, W. Zheng, Highly carbon-doped TiO_2 derived from MXene boosting the photocatalytic hydrogen evolution. ACS Sustain. Chem. Eng. **6**, 13480–13486 (2018). https://doi.org/10.1021/acssuschemeng.8b03406
95. C. Peng, P. Wei, X. Li, Y. Liu, Y. Cao et al., High efficiency photocatalytic hydrogen production over ternary Cu/TiO_2@$Ti_3C_2T_x$ enabled by low-work-function 2D titanium carbide. Nano Energy **53**, 97–107 (2018). https://doi.org/10.1016/j.nanoen.2018.08.040
96. Y. Lu, M. Yao, A. Zhou, Q. Hu, L. Wang, Preparation and photocatalytic performance of Ti_3C_2/TiO_2/CuO ternary nanocomposites. J. Nanomater. **2017**, 1978764 (2017). https://doi.org/10.1155/2017/1978764
97. W. Yuan, L. Cheng, Y. Zhang, H. Wu, L. Zheng, 2D layered Carbon/TiO_2 hybrids derived from Ti_3C_2 MXenes for photocatalytic hydrogen evolution under visible light irradiation. Adv. Mater. Interfaces **4**, 1700577 (2017). https://doi.org/10.1002/admi.201700577
98. J. Low, L. Zhang, T. Tong, B. Shen, J. Yu, TiO_2/MXene Ti_3C_2 composite with excellent photocatalytic CO_2 reduction activity. J. Catal. **361**, 255–266 (2018). https://doi.org/10.1016/j.jcat.2018.03.009
99. T. Su, R. Peng, Z.D. Hood, M. Naguib, I.N. Ivanov et al., One-step synthesis of Nb_2O_5/C/Nb_2C (MXene) composites and their use as photocatalysts for hydrogen evolution. Chemsuschem **11**, 688–699 (2018). https://doi.org/10.1002/cssc.201702317
100. X. Cheng, L. Zu, Y. Jiang, D. Shi, X. Cai, Y. Ni, S. Lin, Y. Qin, A titanium-based photo-fenton bifunctional catalyst of mp-MXene/TiO_{2-x} nanodots for dramatic enhancement of catalytic efficiency in advanced oxidation processes. Chem. Commun. **54**, 11622–11625 (2018). https://doi.org/10.1039/c8cc05866k
101. J. Li, S. Wang, Y. Du, W. Liao, Enhanced photocatalytic performance of TiO_2@C nanosheets derived from two-dimensional Ti_2CT_x. Ceram. Int. **44**, 7042–7046 (2018). https://doi.org/10.1016/j.ceramint.2018.01.139

102. Y. Sun, Y. Sun, X. Meng, Y. Gao, Y. Dall'Agnese et al., Eosin Y-sensitized partially oxidized Ti_3C_2 MXene for photocatalytic hydrogen evolution. Catal. Sci. Technol. **9**, 310–315 (2019). https://doi.org/10.1039/c8cy02240b
103. Y. Li, X. Deng, J. Tian, Z. Liang, H. Cui, Ti_3C_2 MXene-derived Ti_3C_2/TiO_2 nanoflowers for noble-metal-free photocatalytic overall water splitting. Appl. Mater. Today **13**, 217–227 (2018). https://doi.org/10.1016/j.apmt.2018.09.004
104. W. Yuan, L. Cheng, Y. An, S. Lv, H. Wu, X. Fan, Y. Zhang, X. Guo, J. Tang, Laminated hybrid junction of sulfur-doped TiO_2 and a carbon substrate derived from Ti_3C_2 MXenes: toward highly visible light-driven photocatalytic hydrogen evolution. Adv. Sci. **5**, 1700870 (2018). https://doi.org/10.1002/advs.201700870
105. A. Shahzad, K. Rasool, M. Nawaz, W. Miran, J. Jang et al., Heterostructural $TiO_2/Ti_3C_2T_x$ (MXene) for photocatalytic degradation of antiepileptic drug carbamazepine. Chem. Eng. J. **349**, 748–755 (2018). https://doi.org/10.1016/j.cej.2018.05.148
106. Y. Li, Z. Yin, G. Ji, Z. Liang, Y. Xue et al., 2D/2D/2D heterojunction of Ti_3C_2 MXene/MoS_2 nanosheets/TiO_2 nanosheets with exposed (001) facets toward enhanced photocatalytic hydrogen production activity. Appl. Catal. B **246**, 12–20 (2019). https://doi.org/10.1016/j.apcatb.2019.01.051
107. C.J. Zhang, S. Pinilla, N. McEvoy, C.P. Cullen, B. Anasori et al., Oxidation stability of colloidal two-dimensional titanium carbides (MXenes). Chem. Mater. **29**, 4848–4856 (2017). https://doi.org/10.1021/acs.chemmater.7b00745
108. M. Sharma, S. Vaidya, A.K. Ganguli, Enhanced photocatalytic activity of g-C_3N_4-TiO_2 nanocomposites for degradation of Rhodamine B dye. J. Photochem. Photobiol. A **335**, 287–293 (2017). https://doi.org/10.1016/j.jphotochem.2016.12.002
109. L.T. Alameda, P. Moradifar, Z.P. Metzger, N. Alem, R.E. Schaak, Topochemical deintercalation of Al from MoAlB: stepwise etching pathway, layered intergrowth structures, and two-dimensional MBene. J. Am. Chem. Soc. **140**, 8833–8840 (2018). https://doi.org/10.1021/jacs.8b04705

 https://doi.org/10.1007/s40820-019-0309-6